

Occupation time of a system of Brownian particles on the line with steplike initial condition

Ivan N. Burenev, Satya N. Majumdar, and Alberto Rosso
LPTMS, CNRS, Université Paris-Saclay, 91405 Orsay, France

We consider a system of noninteracting Brownian particles on the line with steplike initial condition and study the statistics of the occupation time on the positive half-line. We demonstrate that even at large times, the behavior of the occupation time exhibits long-lasting memory effects of the initialization. Specifically, we calculate the mean and the variance of the occupation time, demonstrating that the memory effects in the variance are determined by a generalized compressibility (or Fano factor), associated with the initial condition. In the particular case of the uncorrelated uniform initial condition we conduct a detailed study of two probability distributions of the occupation time: annealed (averaged over all possible initial configurations) and quenched (for a typical configuration). We show that at large times both the annealed and the quenched distributions admit large deviation form and we compute analytically the associated rate functions. We verify our analytical predictions via numerical simulations using Importance Sampling Monte-Carlo strategy.

I. INTRODUCTION

A classical problem in out-of-equilibrium statistical mechanics is the problem of effusion, i.e. the process in which gas of particles leak from the reservoir through the small hole. In its simplest one-dimensional realization this process can be modeled by initially confining particles within a box and then removing one of the walls. The system is intrinsically out-of-equilibrium which results in nontrivial behaviors even in this seemingly simple case.

One of the peculiar features of such systems lies in their ability to retain an everlasting memory of the initialization. In other words, different initial conditions lead to distinct behaviors and the differences do not fade out with time. For diffusive particles this phenomenon has been observed in various observables, such as total particle current [1, 2]; local time at the origin [3, 4]; displacement of a tracer [5, 6]. Memory effects also persist in more general Gaussian processes [7] and in other systems like run-and-tumble particles [8–10]; Brownian particles with resetting [11, 12] or Jepsen gas [13].

Here we focus exclusively on noninteracting Brownian particles. In this case an important class of observables is so-called Brownian functionals [14]. Denoting by $x_i(t)$ the trajectory of the i -th particle, and by t total time of the process, we define these observables by

$$O \equiv \sum_i \int_0^t V[x_i(t')] dt', \quad (1)$$

where $V[x]$ is an arbitrary function.

It is important to note, that the probability distribution of the functional for an individual particle is inherently dependent on its initial position, hence (1) involves a sum of independent yet *nonidentically* distributed random variables. Consequently the general theory well-developed for identically distributed random variables is inapplicable here. At the same time, initial condition, as was argued in [1], plays a role similar to the realization of the disorder in the theory of disordered systems. Thus there are two natural ways to treat it. The first way is to average over all realizations (“annealed” scheme) and second is to consider a typical initial configuration (“quenched” scheme).

In our previous paper [3] we conducted a study of a specific functional, local time density at the origin, which corresponds to the choice $V[x] = \delta(x)$ in (1). Here we extend the analysis to another observable. Specifically, we opt for $V[x]$ in (1) to be a Heaviside function $V[x] = \theta(x)$

$$T \equiv \sum_i \int_0^t \theta[x_i(t')] dt'. \quad (2)$$

This quantity, usually referred to as occupation (or residence) time on the half-line, characterizes the amount of time particles have spent to the right of the origin.

The single particle counterpart of (2) has been already extensively studied in both mathematics [15–17] and physics literature for various systems. A nonexhaustive list of examples includes diffusion in the Sinai-type potential [18, 19]; fractional Brownian motion [20]; Gaussian Stationary process [21, 22]; run-and-tumble particle [23]; random acceleration model [24]; renewal processes [25, 26]; trap model [27]; continuous-time random walk [28]; coarsening systems [29–31]; heterogeneous diffusion [32]; diffusion with a drift [33, 34]; diffusion with stochastic resetting [35, 36] and also for a class of Gaussian Markov processes [37].

The concept of occupation time arises in very diverse domains. Just to name a few examples, it appears in the context of blinking quantum dots [38]; problems of interface growth [39], spin glasses [40] and stochastic thermodynamics [41]; competitive sports [42] and finance [43].

In this paper we study the statistical properties of the occupation time on the positive half-line (2) for a system of noninteracting Brownian particles on the line with steplike initial condition. Following the approach of [5] we demonstrate that the memory effects in the variance of the occupation time are governed by the generalized compressibility (or Fano factor) of the initial condition. For the particular case of uncorrelated uniform initial condition we study the tails of both quenched and annealed probability distributions at large times. To do this we utilize large deviation theory [44, 45]. We show that both distributions admit the large deviation form and compute corresponding rate functions. All analytical computations are supported by numerical simulations.

Let us stress that the analysis we are to conduct in this paper closely resembles the one presented in [3] for the local time density at the origin. Moreover, since $\delta(x) = \partial_x \theta(x)$, the occupation time and the local time are related in a simple way on the functional level. However, this similarity is, in fact, misleading, and one cannot derive the statistical properties of the occupation time from the known results for the local time density. Therefore to describe statistics of the occupation time precisely, one has to go through the whole machinery of computations. In the present paper we provide these calculations.

The paper is organized as follows. In Section II we introduce the model and the problem we address and present our main results. In Section III, we consider the case of general steplike initial condition. By computing first two cumulants of both quenched and annealed probability distributions, we describe the behavior of the occupation time close to its typical value. We show that the variance depends on the initial condition, and this dependence persists over time. We also show that this memory effect is governed by a single static quantity, known as the generalized compressibility or Fano factor. In Section IV we focus on uncorrelated uniform initial conditions and characterize the tails of the probability distributions by computing corresponding large deviation functions along with their asymptotic expansions. Section V is devoted to numerical simulations. Finally, we conclude in Section VI. In addition, in Appendix A we provide detailed comparison between the results presented in this paper and those obtained in [3] for the local time density at the origin.

II. THE MODEL AND THE MAIN RESULTS

A. The model

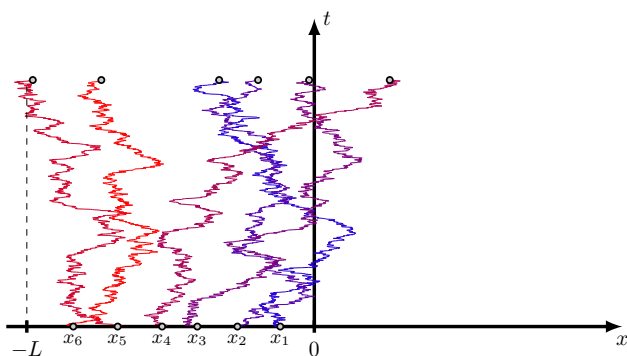


Figure 1. Schematic representation of the Brownian trajectories of for $N = 6$ particles.

Consider a system of N noninteracting Brownian particles on a line initially confined in the box $[-L; 0]$ (see Fig 1). If we denote the coordinate of the i th particle by $x_i(t)$, then the evolution of the system is governed by N independent

Langevin equations

$$\dot{x}_i(t) = \sqrt{2D} \eta_i(t), \quad i = 1, \dots, N \quad (3)$$

where D is the diffusion coefficient and $\eta_i(t)$ is Gaussian white noise with zero mean and unit variance

$$\langle \eta_i(t) \rangle = 0, \quad \langle \eta_i(t) \eta_j(t') \rangle = \delta_{ij} \delta(t - t'). \quad (4)$$

In this paper we study statistical properties of the occupation time (on the positive half-line). Denoting the total time of the process by t , we define this observable as

$$T \equiv \sum_i \int_0^t \theta(x_i(t')) dt' \quad (5)$$

where $\theta(x)$ is a Heaviside θ -function. The quantity (5) measures the amount of time particles have spent to the right of the origin. Note, that in [3] we used the same notation T for the local time density at the origin, but these quantities do not appear together in the main text of the paper, therefore it should not cause any confusion.

Clearly, the occupation time depends on the initial positions of the particles. Therefore, in order for the problem to be well-defined, we need to specify them. In this paper we assume that initial coordinates of the particles are random variables which, in principle, may exhibit correlations. The only requirement is that the marginal probability distribution of a single particle initial coordinate is uniform along the interval $[-L, 0]$.

Since the initial positions of the particles are random, there are two sources of randomness in the system: stochasticity of Brownian trajectories and initial distribution of particles. The latter, as was argued in [1], plays the role, similar to the realization of the disorder in the theory of the disordered systems. Therefore there are two natural ways to treat it. One can either average over all possible realizations of the initial configurations (“annealed” averaging scheme), or consider a typical initial condition (“quenched” averaging scheme). Let us now endow these two schemes with formal definitions.

Consider some fixed initial configuration of particles $\mathbf{x} = (x_1, \dots, x_N)$. Denote by $\mathbb{P}[T, t | \mathbf{x}]$ the probability that at the observation time t the total occupation time is equal to T and by $\langle e^{-pT} \rangle_{\mathbf{x}}$ its Laplace transform

$$\langle e^{-pT} \rangle_{\mathbf{x}} \equiv \int_0^{Nt} dT e^{-pT} \mathbb{P}[T, t | \mathbf{x}]. \quad (6)$$

Then annealed and quenched probability distributions are defined as

$$\int_0^{Nt} dT e^{-pT} \mathbb{P}_{\text{an}}[T, t] \equiv \overline{\langle e^{-pT} \rangle_{\mathbf{x}}}, \quad (7)$$

$$\int_0^{Nt} dT e^{-pT} \mathbb{P}_{\text{qu}}[T, t] \equiv \exp \left[\overline{\log \langle e^{-pT} \rangle_{\mathbf{x}}} \right] \quad (8)$$

Here and subsequently bar $\overline{\dots}$ denotes averaging over realizations of the initial conditions and brackets $\langle \dots \rangle_{\mathbf{x}}$ stand for

averaging over Brownian trajectories with initial configuration \mathbf{x} kept fixed. The upper limit in the Laplace transforms is due to the fact that the occupation time for a single particle is bounded by the total observation time.

The aim of this paper is to study the statistics of the occupation time (5) at large times in the thermodynamic limit, i.e. the limit in which $N, L \rightarrow \infty$ with their ratio $\bar{\rho} = N/L$ being fixed. In particular we shall study two probability distributions of the occupation time: annealed $\mathbb{P}_{\text{an}}[T, t]$ and quenched $\mathbb{P}_{\text{qu}}[T, t]$, defined by (7) and (8) respectively.

B. The main results

The probability distribution of the occupation time close to its typical value has a Gaussian form which can be characterized by the mean and the variance. We compute them for the general steplike initial condition in which initial coordinates may be correlated.

First, we compute the mean value of the occupation time

$$\overline{\langle T \rangle}_{\mathbf{x}} = \frac{2}{3} \sqrt{\frac{D}{\pi}} \bar{\rho} t^{3/2}. \quad (9)$$

Expression (9) holds for both annealed and quenched probability distributions. However the variances differ. For the quenched variance, which is defined in accordance with (8) as

$$\text{Var}_{\text{qu}}[T] = \overline{\langle T^2 \rangle}_{\mathbf{x}} - \overline{\langle T \rangle}_{\mathbf{x}}^2, \quad (10)$$

we find the explicit form

$$\text{Var}_{\text{qu}}[T] = \frac{8(\sqrt{2}-1)}{15} \sqrt{\frac{D}{\pi}} \bar{\rho} t^{5/2}. \quad (11)$$

We emphasize that results (9) and (11) hold for any time t . Another observation we can make from (11) is that the quenched variance depends only on the average density of particles in the initial configuration and has no memory of possible correlations whatsoever.

The annealed variance according to (7) is defined as

$$\text{Var}_{\text{an}}[T] = \overline{\langle T^2 \rangle}_{\mathbf{x}} - \overline{\langle T \rangle}_{\mathbf{x}}^2. \quad (12)$$

We find that at large times its behavior reads

$$\text{Var}_{\text{an}}[T] \underset{t \rightarrow \infty}{\simeq} \left[\frac{2}{5} + \frac{2(4\sqrt{2}-7)}{15} (1 - \alpha_{\text{ic}}) \right] \sqrt{\frac{D}{\pi}} \bar{\rho} t^{5/2}, \quad (13)$$

where α_{ic} denotes the Fano factor (generalized compressibility) of the initial condition

$$\alpha_{\text{ic}} \equiv \lim_{\ell \rightarrow \infty} \frac{\text{Var}[n(\ell)]}{n(\ell)}. \quad (14)$$

Here $n(\ell)$ stands for the number of particles initially located in the segment $[-\ell, 0]$.

It is clear from (13), that the annealed variance does indeed depend on the initialization. However, all the dependence is encoded in a single static quantity α_{ic} . In other words, if we initialize the systems in two different ways — by drawing the initial configurations from either distribution $p_1(\mathbf{x})$ or $p_2(\mathbf{x})$ with different Fano factor — then we can distinguish between these initialization protocols by looking at the annealed variance of the occupation time. This is exactly what we mean by the memory of the initial condition.

Let us take a closer look at two particular cases. First is the hyperuniform initial condition, i.e. the initial condition in which the ratio $\ell^{-1} \text{Var}[n(\ell)] \rightarrow 0$ as $\ell \rightarrow 0$. In this case α_{ic} is equal to zero. Consequently

$$\alpha_{\text{ic}} = 0 : \quad \text{Var}_{\text{an}}[T] \underset{t \rightarrow \infty}{\simeq} \frac{8(\sqrt{2}-1)}{15} \sqrt{\frac{D}{\pi}} \bar{\rho} t^{5/2}. \quad (15)$$

Comparing (15) with (11) suggests, that the “typical” initial configuration, as mentioned when handwavingly defining the quenched probability distribution, is essentially a configuration drawn from a hyperuniform distribution (see Sec III B for more details).

Another important special case is uncorrelated uniform initial condition, the scenario in which initial positions of particles are drawn from the uniform distribution independently. Since particles do not interact, uncorrelated uniform distribution is essentially the equilibrium distribution and therefore it is a very natural choice for the initial condition. In this case, the distribution of the number of particles in a segment $n(\ell)$ is a Poisson distribution. Therefore the mean and the variance entering (14) are the same, hence $\alpha_{\text{ic}} = 1$ and we have

$$\alpha_{\text{ic}} = 1 : \quad \text{Var}_{\text{an}}[T] \underset{t \rightarrow \infty}{\simeq} \frac{2}{5} \sqrt{\frac{D}{\pi}} \bar{\rho} t^{5/2}. \quad (16)$$

Actually, for the uncorrelated uniform initial condition, expression (16) is exact for all times and not only in the limit $t \rightarrow \infty$ (see III B for details). In particular this implies, that

$$\text{uncorrelated uniform:} \quad \frac{\text{Var}_{\text{qu}}[T]}{\text{Var}_{\text{an}}[T]} = 4 \frac{\sqrt{2}-1}{3} < 1 \quad (17)$$

and this ratio *does not depend on time*.

To explore the tails of the probability distributions we resort to the large deviation formalism [44, 45]. We find that the probability distributions admit the large deviation forms

$$\mathbb{P}_{\text{an}}[T, t] \simeq \exp \left[-\bar{\rho} \sqrt{4Dt} \Phi_{\text{an}}(\tau) \right], \quad (18)$$

$$\mathbb{P}_{\text{qu}}[T, t] \simeq \exp \left[-\bar{\rho} \sqrt{4Dt} \Phi_{\text{qu}}(\tau) \right], \quad (19)$$

where

$$\tau \equiv \frac{T}{t^{3/2}} \frac{1}{\bar{\rho} \sqrt{4D}}. \quad (20)$$

As we show in Sec. III B, quenched rate function $\Phi_{\text{qu}}(\tau)$ is the same for all steplike initial conditions. Annealed rate function $\Phi_{\text{an}}(\tau)$, on the other hand, is more subtle, and is different for different initial conditions. Therefore we restrict ourselves to the case of uncorrelated uniform initial condition.

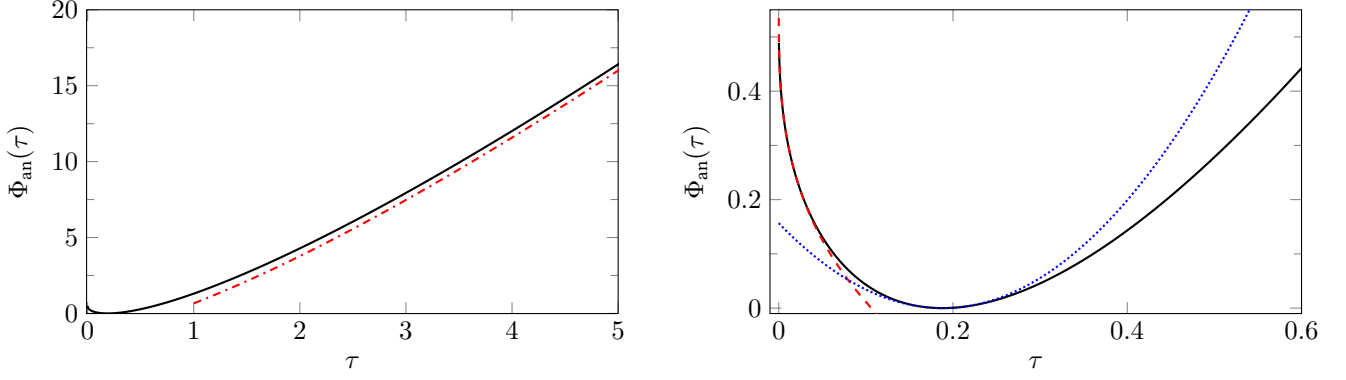


Figure 2. Large deviation function in the annealed case and its asymptotic expansions. In the left panel τ has a larger range, while in the right panel, we zoom in around the minimum of $\Phi_{\text{an}}(\tau)$ reached at $\tau = \tau_{\text{typ}} = \frac{1}{3\sqrt{\pi}}$. On both panels the solid lines correspond to the large deviation function computed in Mathematica from (21) and (22). Dashed, dotted and dash-dotted lines are asymptotic behaviors of $\Phi_{\text{an}}(\tau)$ in (23) for small, typical and large values of rescaled occupation time τ (20) respectively.

For the uncorrelated uniform initial condition we find that the annealed rate function $\Phi_{\text{an}}(\tau)$ is given by an inverse Legendre transform

$$\Phi_{\text{an}}(\tau) = \max_q (-q\tau + \phi_{\text{an}}(q)) \quad (21)$$

with

$$\phi_{\text{an}}(q) = \frac{1}{\sqrt{\pi}} - \frac{1}{\sqrt{4q}} \operatorname{erf}(\sqrt{q}). \quad (22)$$

Expression (22) together with (21) provide parametric representation of $\Phi_{\text{an}}(\tau)$ (see Fig 2). Analyzing these two expressions we extract leading asymptotic behaviors of $\Phi_{\text{an}}(\tau)$

$$\Phi_{\text{an}}(\tau) \sim \begin{cases} \frac{1}{\sqrt{\pi}} - \frac{3}{2} \left(\frac{\tau}{2}\right)^{1/3}, & \tau \rightarrow 0, \\ \frac{5}{2} \sqrt{\pi} \left(\tau - \frac{1}{3\sqrt{\pi}}\right)^2, & \tau \rightarrow \frac{1}{3\sqrt{\pi}}, \\ \tau \left(\mu \log [2\tau\sqrt{\pi}] - \frac{1}{\mu}\right), & \tau \rightarrow \infty, \end{cases} \quad (23)$$

where

$$\mu \equiv 1 + \frac{\log \log [2\tau\sqrt{\pi}]}{\log [2\tau\sqrt{\pi}]}. \quad (24)$$

Asymptotic expansion (23) along with the large deviation form (18) imply that close to the typical value of the occupation time, annealed probability distribution is given by

$$\mathbb{P}_{\text{an}}[T, t] \simeq \exp \left[-\frac{1}{2} \left(\frac{T - T_{\text{typ}}}{\sigma_{\text{an}}} \right)^2 \right], \quad T \rightarrow T_{\text{typ}} \quad (25)$$

with

$$T_{\text{typ}} = \frac{2}{3} \sqrt{\frac{D}{\pi}} \bar{\rho} t^{3/2}, \quad \sigma_{\text{an}}^2 = \frac{2}{5} \sqrt{\frac{D}{\pi}} \bar{\rho} t^{5/2}. \quad (26)$$

This is exactly the result we anticipate from (9) and (16).

For the quenched rate function $\Phi_{\text{qu}}(\tau)$ we obtain similar representation. Namely

$$\Phi_{\text{qu}}(\tau) = \max_q (-q\tau + \phi_{\text{qu}}(q)) \quad (27)$$

where

$$\phi_{\text{qu}}(q) = - \int_0^\infty dy \log \left[\operatorname{erf}(y) + \frac{1}{\pi} \int_0^1 d\xi \frac{e^{-q\xi - \frac{y^2}{1-\xi}}}{\sqrt{\xi(1-\xi)}} \right]. \quad (28)$$

Expressions (27) and (28) give us parametric representation of the quenched rate function $\Phi_{\text{qu}}(\tau)$ (see Fig 3) and allows us to find the asymptotic behaviors

$$\Phi_{\text{qu}}(\tau) \sim \begin{cases} \phi_\infty - \frac{1 + \frac{1}{2} \log \nu + \frac{1}{3} \log \log \nu}{\frac{2}{\sqrt{\pi}} (\nu \log \nu)^{1/3}}, & \tau \rightarrow 0, \\ \frac{1}{2} \frac{15\sqrt{\pi}}{4(\sqrt{2}-1)} \left(\tau - \frac{1}{3\sqrt{\pi}}\right)^2, & \tau \rightarrow \frac{1}{3\sqrt{\pi}}, \\ \left(\frac{4}{3}\tau\right)^3, & \tau \rightarrow \infty, \end{cases} \quad (29)$$

where

$$\nu = \frac{\pi^{3/2}}{12\tau}, \quad \phi_\infty = - \int_0^\infty \log [\operatorname{erf}(y)] dy \approx 1.03. \quad (30)$$

Similarly to the annealed case, from (29) and (19) it is clear that close to the typical value of the occupation time

$$\mathbb{P}_{\text{qu}}[T, t] \simeq \exp \left[-\frac{1}{2} \left(\frac{T - T_{\text{typ}}}{\sigma_{\text{qu}}} \right)^2 \right], \quad T \rightarrow T_{\text{typ}} \quad (31)$$

where

$$T_{\text{typ}} = \frac{2}{3} \sqrt{\frac{D}{\pi}} \bar{\rho} t^{3/2}, \quad \sigma_{\text{qu}}^2 = \frac{8(\sqrt{2}-1)}{15} \sqrt{\frac{D}{\pi}} \bar{\rho} t^{5/2}. \quad (32)$$

which indeed matches with the mean (9) and the variance (11).

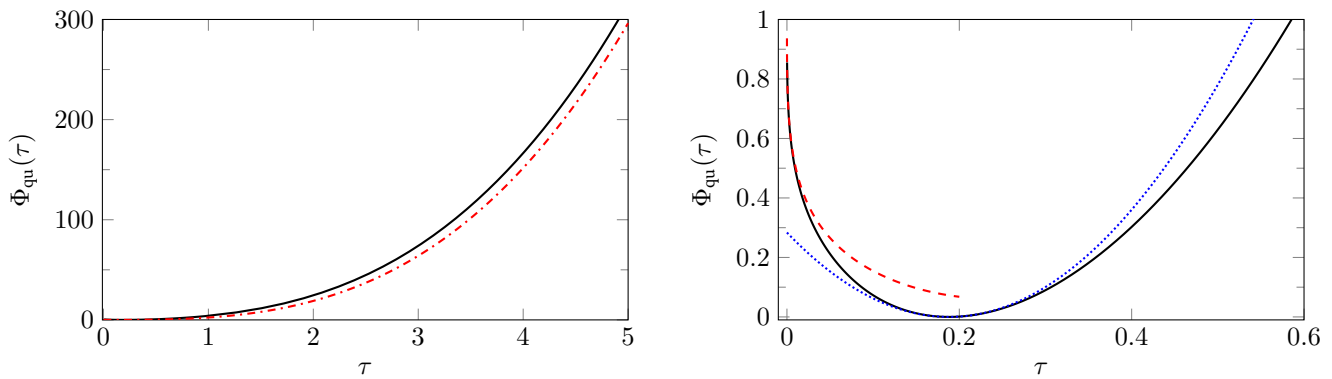


Figure 3. Large deviation function in the quenched case and its asymptotic expansions. In the left panel τ has a larger range, while in the right panel, we zoom in around the minimum of $\Phi_{\text{qu}}(\tau)$ reached at $\tau = \tau_{\text{typ}} = \frac{1}{3\sqrt{\pi}}$. On both panels the solid lines correspond to the large deviation function computed in Mathematica from (27) and (28). Dashed, dotted and dash-dotted lines are asymptotic behaviors of $\Phi_{\text{qu}}(\tau)$ in (29) for small, typical and large values of rescaled occupation time τ (20) respectively.

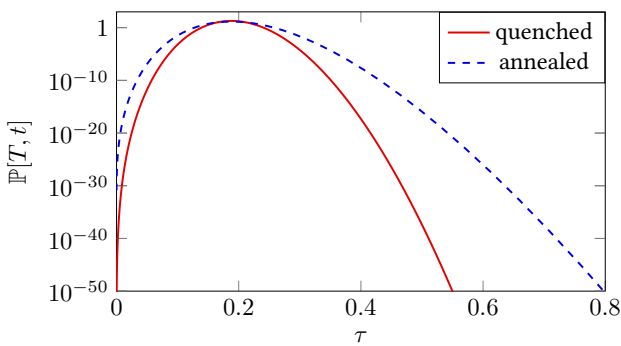


Figure 4. Quenched (solid) and annealed (dashed) probability distributions obtained from (19) and (18) respectively. In this plot we use $t = 10000$, $D = 1/2$, $\bar{\rho} = 1$.

Note that the annealed and quenched probability distributions are very different (see Fig 4 for the comparison). For example, the probabilities that $T = 0$, i.e. the probabilities that no particle have reached the origin up to the observation time t , in both cases are stretched exponentials

$$\mathbb{P}_{\text{an}}[0, t] \sim e^{-\theta_{\text{an}} \bar{\rho} \sqrt{4Dt}}, \quad \mathbb{P}_{\text{qu}}[0, t] \sim e^{-\theta_{\text{qu}} \bar{\rho} \sqrt{4Dt}}, \quad (33)$$

but the constants are different. Namely

$$\theta_{\text{an}} = \frac{1}{\sqrt{\pi}} \approx 0.56, \quad \theta_{\text{qu}} = \phi_{\infty} \approx 1.03. \quad (34)$$

This difference is due to the atypical initial conditions. The annealed probability distribution takes into account initial configurations in which particles are far from the origin and hence they require more time to reach it, which leads to higher probability of survival. Such initial conditions are indeed the atypical ones and therefore they do not contribute to the quenched probability distribution.

In fact, survival probabilities (33) naturally appear in the context of target problems (see [46] for a review) and both

constants in (34) can be computed in a much simpler way [47]. Here we obtain them as byproducts.

The behaviors of the quenched and annealed distributions at atypically large occupation times also differ. Asymptotic expansions (23) and (29) imply that

$$\mathbb{P}_{\text{an}}[T, t] \sim \exp \left[-\frac{1}{2} \frac{T}{t} \log \left(\frac{1}{t^3 D \bar{\rho}^2} T^2 \right) \right], \quad T \gg T_{\text{typ}}, \quad (35)$$

$$\mathbb{P}_{\text{qu}}[T, t] \sim \exp \left[-\frac{16}{27} \frac{T}{t} \left(\frac{1}{t^3 D \bar{\rho}^2} T^2 \right) \right], \quad T \gg T_{\text{typ}}. \quad (36)$$

Thus, the quenched probability distribution decay much faster than the annealed one. This is due to the atypical initial configurations, in which particles are concentrated in the vicinity of the origin. Since it does not take much time for these particles to reach the origin, they contribute to the atypically large values of the occupation time.

III. THE MEAN AND THE VARIANCE

Close to the typical value, we expect the probability distribution of the occupation time to be Gaussian and hence we can describe it by the mean and the variance. In this section we compute them for general steplike initial condition in both annealed and quenched averaging schemes.

A. One particle

Let us first consider the case of the individual particle. In the case of simple Brownian motion the probability distribution $\mathbb{P}[T, t | x]$ of the occupation time T can be found e.g. in [17] (p. 162 therein), and for a pedagogical derivation of this result we refer the reader to [14]. If the particle starts at $x(0) = x \leq 0$, then the probability distribution $\mathbb{P}[T, t | x]$

reads

$$\begin{aligned} \mathbb{P}[T, t | x] &= \operatorname{erf} \left[\frac{|x|}{\sqrt{4Dt}} \right] \delta(T) \\ &+ \frac{1}{\pi} \frac{1}{\sqrt{T(t-T)}} \exp \left[-\frac{x^2}{4D(t-T)} \right], \quad x \leq 0, \end{aligned} \quad (37)$$

where

$$\operatorname{erf}(z) = \frac{2}{\sqrt{\pi}} \int_0^z e^{-s^2} ds. \quad (38)$$

Note, that if the particle starts at the origin, then (37) simplifies into the famous Lévy's arcsine law [48]

$$\mathbb{P}[T, t | x = 0] = \frac{1}{\pi} \frac{1}{\sqrt{T(t-T)}}. \quad (39)$$

The first term in (37) comes from the trajectories that have not reached the origin up to time t , and is nothing but the survival probability of an individual particle.

We should stress, that the expression (37) is valid only when $x \leq 0$. But since this is exactly the case we are interested in, to simplify the notation we shall not emphasize this anymore.

We will also need the Laplace transform of the $\mathbb{P}[T, t | x]$ which is defined in a usual way as

$$\langle e^{-pT} \rangle_x \equiv \int_{0-}^t e^{-pT} \mathbb{P}[T, t | x] dT. \quad (40)$$

Since the occupation time cannot be larger than t , the probability measure is supported on $[0, t]$ and hence the upper limit in the integral above. Using the explicit form (37) of the probability distribution $\mathbb{P}[T, t | x]$ we obtain

$$\begin{aligned} \langle e^{-pT} \rangle_x &= \operatorname{erf} \left[\frac{|x|}{\sqrt{4Dt}} \right] \\ &+ \frac{1}{\pi} \int_0^1 d\xi \frac{e^{-pt\xi}}{\sqrt{\xi(1-\xi)}} \exp \left[-\frac{x^2}{4Dt} \frac{1}{(1-\xi)} \right]. \end{aligned} \quad (41)$$

The integral in (41) has no explicit expression in terms of elementary functions, but nevertheless it provides us a lot of information. For example the moments of the occupation time are given by

$$\langle T^n \rangle_x = t^n \frac{1}{\pi} \int_0^1 d\xi \frac{\xi^n}{\sqrt{\xi(1-\xi)}} \exp \left[-\frac{x^2}{4Dt} \frac{1}{(1-\xi)} \right]. \quad (42)$$

After the change of variables $\xi = \frac{y}{y+1}$ and rescaling of the coordinate $z = \frac{x^2}{4Dt}$ expression (42) transforms into

$$\langle T^n \rangle_{x=-\sqrt{4Dt}z} = t^n e^{-z} \frac{\Gamma(n + \frac{1}{2})}{\pi} U \left(n + \frac{1}{2}, \frac{1}{2}; z \right), \quad (43)$$

where $\Gamma(a)$ is Euler gamma function and $U(a, b; z)$ denotes the confluent hypergeometric function of the second kind [49]

$$U(a, b; z) \equiv \frac{1}{\Gamma(a)} \int_0^\infty ds e^{-zs} s^{a-1} (s+1)^{b-a-1} \quad (44)$$

From (44) it follows that $U(a, b; z)$ satisfies a recurrence relation

$$U(a+1, b; z) = \frac{z^{1-a}}{a(a-b+1)} \frac{d}{dz} \left[z^a U(a, b; z) \right]. \quad (45)$$

In addition, one can easily check that

$$U \left(\frac{1}{2}, \frac{1}{2}; z \right) = \sqrt{\pi} e^z (1 - \operatorname{erf}(\sqrt{z})). \quad (46)$$

Combining (46) with recurrence relation (45) and then using (43) we can find all the moments of the occupation time. In particular the first two moments are

$$\langle T \rangle_{x=-\sqrt{4Dt}z} = t \left[\left(\frac{1}{2} + z \right) \operatorname{erfc}(\sqrt{z}) - \frac{\sqrt{z} e^{-z}}{\sqrt{\pi}} \right], \quad (47)$$

$$\begin{aligned} \langle T^2 \rangle_{x=-\sqrt{4Dt}z} &= t^2 \left(\frac{3}{8} + \frac{3}{2}z + \frac{1}{2}z^2 \right) \operatorname{erfc}(\sqrt{z}) \\ &- t^2 \left(\frac{1}{2}z + \frac{5}{4} \right) \frac{\sqrt{z} e^{-z}}{\sqrt{\pi}} \end{aligned} \quad (48)$$

where $\operatorname{erfc}(z) = 1 - \operatorname{erf}(z)$. From (47) and (48) we extract large time behavior for the mean and the variance of the occupation time. At large times

$$z = \frac{x^2}{4Dt} \rightarrow 0, \quad t \rightarrow \infty \quad (49)$$

and hence

$$\langle T \rangle_x \sim \frac{1}{2} t, \quad \langle T^2 \rangle_x - \langle T \rangle_x^2 \sim \frac{1}{8} t^2, \quad t \rightarrow \infty. \quad (50)$$

B. System of particles

Now we proceed to the system of N Brownian particles initially located to the left of the origin and compute the mean and the variance of the occupation time. But first of all we shall specify initial conditions more precisely.

Denoting by x_i the position of the i -th particle at $t = 0$, we define the empirical density of the initial condition as

$$\hat{\rho}(y | \mathbf{x}) \equiv \sum_i \delta(x_i - y). \quad (51)$$

Now all the information about the initial configuration is encoded in $\hat{\rho}(y | \mathbf{x})$. In what follows, we restrict ourselves to the particular type of the initial condition, that is we assume that the initial configuration of the particles was obtained from the translational invariant distribution on the real line by removing all particles on the positive half-line. This assumption essentially implies two things. First, the average density is a constant to the left of the origin and zero to the right

$$\overline{\hat{\rho}(y | \mathbf{x})} = \bar{\rho} \theta(-y). \quad (52)$$

Second, two point correlation function $C(y_1, y_2)$ of the initial condition

$$C(y_1, y_2) \equiv \overline{\hat{\rho}(y_1 | \mathbf{x}) \hat{\rho}(y_2 | \mathbf{x})} - \bar{\rho}^2 \quad (53)$$

depends only on the difference $(y_1 - y_2)$

$$C(y_1, y_2) = \bar{\rho} \theta(-y_1) \theta(-y_2) C(y_1 - y_2). \quad (54)$$

Note that we can already guess the scaling behavior of both the mean and the variance. Indeed, the typical displacement of a Brownian particle is proportional to \sqrt{Dt} . Consequently, the particles that have reached the origin up to time t are those that were initially located within the segment $[-\sqrt{Dt}, 0]$. Since there are approximately $\bar{\rho} \sqrt{Dt}$ such particles, and contribution of each particle to the mean value of the occupation time is proportional to t (50), we expect the mean value of the total occupation time to scale as $\sqrt{t} \cdot t = t^{3/2}$. Similarly, we expect the variance to scale as $\sqrt{t} \cdot t^2 = t^{5/2}$. Having this heuristic argument in mind, we proceed to the rigorous computation.

The mean value of the occupation time for a given initial configuration \mathbf{x} in terms of the empirical density reads

$$\langle T \rangle_{\mathbf{x}} = \int_{-\infty}^{\infty} dy \hat{\rho}(y | \mathbf{x}) \langle T \rangle_y, \quad (55)$$

where $\langle T \rangle_y$ denotes the mean value of the occupation time of a single particle starting at y which is given by (47). Averaging (55) over initial conditions we get

$$\overline{\langle T \rangle_{\mathbf{x}}} = \int_{-\infty}^{\infty} dy \overline{\hat{\rho}(y | \mathbf{x})} \langle T \rangle_y. \quad (56)$$

Combining (56) with (52) we obtain

$$\overline{\langle T \rangle_{\mathbf{x}}} = \bar{\rho} \int_{-\infty}^0 dy \langle T \rangle_y. \quad (57)$$

Recalling (47) and after straightforward computation we arrive at

$$\overline{\langle T \rangle_{\mathbf{x}}} = \frac{2}{3} \sqrt{\frac{D}{\pi}} \bar{\rho} t^{3/2}. \quad (58)$$

This is the result stated in (9). The mean value depends only on the average density of the particles and is the same for both quenched and annealed distributions. Let us now proceed to the computation of the variances

We start with the quenched distribution. According to (8), the quenched variance is given by

$$\text{Var}_{\text{qu}}[T] = \overline{\langle T^2 \rangle_{\mathbf{x}}} - \overline{\langle T \rangle_{\mathbf{x}}}^2 \quad (59)$$

or in terms of the empirical density

$$\text{Var}_{\text{qu}}[T] = \int_{-\infty}^{\infty} dy \overline{\hat{\rho}(y | \mathbf{x})} \left[\langle T^2 \rangle_y - \langle T \rangle_y^2 \right]. \quad (60)$$

Due to (52), averaging over initial conditions yields

$$\text{Var}_{\text{qu}}[T] = \bar{\rho} \int_{-\infty}^0 dy \left[\langle T^2 \rangle_y - \langle T \rangle_y^2 \right]. \quad (61)$$

Substituting (47) and (48) into (61) we get

$$\text{Var}_{\text{qu}}[T] = \frac{8(\sqrt{2}-1)}{15} \sqrt{\frac{D}{\pi}} \bar{\rho} t^{5/2}. \quad (62)$$

This is exactly the result (11).

Note that the quenched variance depends only on the average density of particles in the initial configuration. In fact, the same is true for the full probability distribution $\mathbb{P}_{\text{qu}}[T, t]$. It becomes clear if we rewrite its definition (8) in terms of the empirical density (51). Since there is no interaction we have

$$\log \langle e^{-pT} \rangle_{\mathbf{x}} = \int_{-\infty}^{\infty} dy \hat{\rho}(y | \mathbf{x}) \log \langle e^{-pT} \rangle_y \quad (63)$$

hence

$$\overline{\log \langle e^{-pT} \rangle_{\mathbf{x}}} = \bar{\rho} \int_{-\infty}^0 dy \log \langle e^{-pT} \rangle_y \quad (64)$$

and therefore

$$\int_{0-}^{Nt} dT e^{-pT} \mathbb{P}_{\text{qu}}[T, t] = \exp \left[\bar{\rho} \int_{-\infty}^0 dy \log \langle e^{-pT} \rangle_y \right]. \quad (65)$$

Now we advance to the annealed probability distribution. In accordance with (7) its variance is

$$\text{Var}_{\text{an}}[T] = \overline{\langle T^2 \rangle_{\mathbf{x}}} - \overline{\langle T \rangle_{\mathbf{x}}}^2. \quad (66)$$

Following the procedure introduced in [5] (see also [7] Sec. IV) we formally rewrite (66) as a sum of two terms

$$\begin{aligned} \text{Var}_{\text{an}}[T] &= \left[\overline{\langle T^2 \rangle_{\mathbf{x}}} - \overline{\langle T \rangle_{\mathbf{x}}}^2 \right] + \left[\overline{\langle T \rangle_{\mathbf{x}}^2} - \overline{\langle T \rangle_{\mathbf{x}}}^2 \right] \\ &= \text{Var}_{\text{qu}}[T] + \text{Var}_{\text{ic}}[T]. \end{aligned} \quad (67)$$

The first term in (67) is the quenched variance (59) and all dependence of possible correlations in the initial condition is encoded solely in the second term

$$\text{Var}_{\text{ic}}[T] \equiv \overline{\langle T \rangle_{\mathbf{x}}^2} - \overline{\langle T \rangle_{\mathbf{x}}}^2. \quad (68)$$

To express $\text{Var}_{\text{ic}}[T]$ in terms of the empirical density (51) we note that

$$\overline{\langle T \rangle_{\mathbf{x}}^2} = \int_{-\infty}^{\infty} dy \int_{-\infty}^{\infty} dy' \overline{\hat{\rho}(y | \mathbf{x}) \hat{\rho}(y' | \mathbf{x})} \langle T \rangle_y \langle T \rangle_{y'} \quad (69)$$

and

$$\overline{\langle T \rangle_{\mathbf{x}}^2} = \bar{\rho}^2 \int_{-\infty}^0 dy \langle T \rangle_y \int_{-\infty}^0 dy' \langle T \rangle_{y'}. \quad (70)$$

Substituting (70) and (69) into (68) we express $\text{Var}_{\text{ic}}[T]$ in terms of two point correlation function (53) as

$$\text{Var}_{\text{ic}}[T] = \bar{\rho} \int_{-\infty}^0 dy \int_{-\infty}^0 dy' \langle T \rangle_y \langle T \rangle_{y'} C(y - y'). \quad (71)$$

To proceed further we should either specify initial condition and provide the exact form of the $C(y - y')$ or, alternatively,

we can study the large time limit and compute (71) as $t \rightarrow \infty$. The latter can be done by introducing the Fourier transform of the two-point correlation function

$$C(y) = \frac{1}{2\pi} \int_{-\infty}^{\infty} dq e^{iqy} S(q). \quad (72)$$

Then (71) turns into

$$\text{Var}_{\text{ic}}[T] = \bar{\rho} \int_{-\infty}^0 dy \int_{-\infty}^0 dy' \langle T \rangle_y \langle T \rangle_{y'} \frac{1}{2\pi} \int_{-\infty}^{\infty} dq S(q) e^{iq(y-y')}. \quad (73)$$

In the limit $t \rightarrow \infty$ the integral over q is essentially a δ -function. Indeed, if we rescale the variables of the integration in (73) as $y = 4Dt \tilde{y}$, $y' = 4Dt \tilde{y}'$, $q = \frac{p}{4Dt}$, then the integral over q transforms into

$$\frac{1}{2\pi} \int_{-\infty}^{\infty} dp S\left(\frac{p}{4Dt}\right) e^{ip(\tilde{y}-\tilde{y}')} \underset{t \rightarrow \infty}{\simeq} S(0) \delta(\tilde{y}-\tilde{y}') \quad (74)$$

where we used a representation

$$\delta(\tilde{y}-\tilde{y}') = \frac{1}{2\pi} \int_{-\infty}^{\infty} dp e^{ip(\tilde{y}-\tilde{y}')}. \quad (75)$$

Due to (74) at large times (73) simplifies into

$$\text{Var}_{\text{ic}}[T] \simeq \bar{\rho} S(0) \int_{-\infty}^0 dy \langle T \rangle_y^2, \quad t \rightarrow \infty \quad (76)$$

and using (47) we arrive at

$$\text{Var}_{\text{ic}}[T] \simeq S(0) \frac{2(7-4\sqrt{2})}{15} \sqrt{\frac{D}{\pi}} \bar{\rho} t^{5/2}, \quad t \rightarrow \infty. \quad (77)$$

The quantity $S(0)$ is exactly the Fano factor defined in (14). To see this, we express $n(\ell)$ in terms of the empirical density

$$n(\ell) = \int_{-\ell}^0 dy \hat{\rho}(y | \mathbf{x}). \quad (78)$$

hence

$$\overline{n(\ell)} \sim \ell \bar{\rho}, \quad \ell \rightarrow \infty. \quad (79)$$

Similarly for the variance

$$\text{Var}[n(\ell)] = \int_{-\ell}^0 dy \int_{-\ell}^0 dy' \left[\overline{\hat{\rho}(y | \mathbf{x}) \hat{\rho}(y' | \mathbf{x})} - \bar{\rho}^2 \right] \quad (80)$$

the integrand is nothing but a two-point correlation function (53). Using the Fourier transform (72) after rescaling $p = q\ell$, $y = \tilde{y}\ell$, $y' = \tilde{y}'\ell$ we get

$$\text{Var}[n(\ell)] = \bar{\rho} \ell \int_{-1}^0 d\tilde{y} \int_{-1}^0 d\tilde{y}' \int_{-\infty}^{\infty} \frac{dp}{2\pi} e^{ip(\tilde{y}-\tilde{y}')} S\left(\frac{p}{\ell}\right) \quad (81)$$

which in the limit $\ell \rightarrow \infty$ reduces to

$$\text{Var}[n(\ell)] \sim \bar{\rho} \ell \int_{-1}^0 d\tilde{y} \int_{-1}^0 d\tilde{y}' \delta(\tilde{y}-\tilde{y}') S(0) \quad (82)$$

hence

$$\text{Var}[n(\ell)] \sim \bar{\rho} \ell S(0) \quad \ell \rightarrow \infty \quad (83)$$

and

$$\alpha_{\text{ic}} \equiv \lim_{\ell \rightarrow \infty} \frac{\text{Var}[n(\ell)]}{n(\ell)} = S(0). \quad (84)$$

Having expressions (62) and (77) for both terms in (67) we combine them together arriving at the result stated in (13), i.e.

$$\text{Var}_{\text{an}}[T] \underset{t \rightarrow \infty}{\simeq} \left[\frac{2}{5} + \frac{2(4\sqrt{2}-7)}{15} (1 - \alpha_{\text{ic}}) \right] \sqrt{\frac{D}{\pi}} \bar{\rho} t^{5/2}. \quad (85)$$

As we have mentioned, instead of taking the limit $t \rightarrow \infty$ in (71) we can choose a particular initial condition. For example, if we draw initial coordinates independently from the uniform distribution, then two point correlation function is just a δ -function

$$C(y_1, y_2) = \bar{\rho} \theta(-y_1) \theta(-y_2) \delta(y_1 - y_2). \quad (86)$$

Then $\alpha_{\text{ic}} = S(0) = 1$ and (71) simplifies into

$$\text{uncorr. uniform: } \text{Var}_{\text{ic}}[T] = \bar{\rho} \int_{-\infty}^0 dy \langle T \rangle_y^2 \quad (87)$$

hence

$$\text{uncorr. uniform: } \text{Var}_{\text{ic}}[T] = \frac{2(7-4\sqrt{2})}{15} \sqrt{\frac{D}{\pi}} \bar{\rho} t^{5/2}. \quad (88)$$

and for the annealed variance we get

$$\text{uncorr. uniform: } \text{Var}_{\text{an}}[T] = \frac{2}{5} \sqrt{\frac{D}{\pi}} \bar{\rho} t^{5/2}. \quad (89)$$

We stress that for the uncorrelated uniform initial condition, expression (89) is valid at any time whereas (85) is the behavior at large times.

As a final remark let us briefly comment on the physical meaning of the quenched probability distribution. At this point, we have already mentioned a couple of times that the quenched probability distribution corresponds to fixing the initial configuration of particles to be a ‘‘typical’’ one. But what are these ‘‘typical’’ configurations exactly? Comparing (85) with (62) suggests, that ‘‘typical’’ configurations are those, drawn from the probability distribution with $\alpha_{\text{ic}} = 0$. In fact, we can point out the ‘‘typical’’ initial conditions more precisely. Namely, if we consider a fixed initial configuration, such that $x_i(0)$ is confined within the segment χ_i

$$\chi_i \equiv \left[-\frac{i}{\bar{\rho}}, -\frac{i-1}{\bar{\rho}} \right], \quad (90)$$

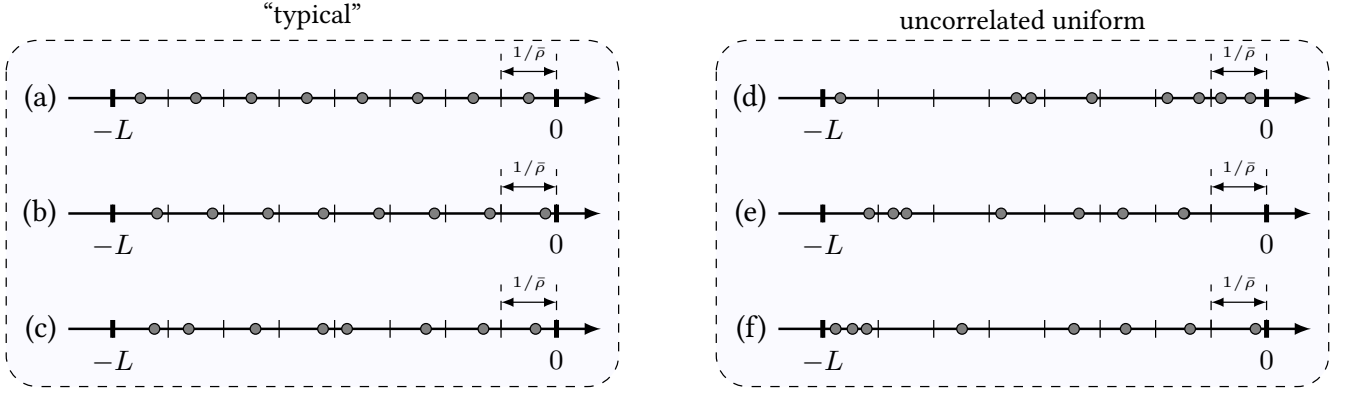


Figure 5. Examples of typical initial configurations (a)-(c). For the comparison, we provide three initial configurations (d)-(f) drawn from the uncorrelated uniform probability distribution.

and study the probability distribution of the occupation time, then at large observation time, the resulting distribution will be the same as the quenched one $\mathbb{P}_{\text{qu}}[T, t]$ defined in (8). In other words all these configurations are “typical” (see Fig. 5). The rigorous proof of this statement is essentially the same as the one we have performed in [3] for the local time density at the origin (see Appendix B therein), therefore, to avoid burying the reader under technical details, we do not provide the derivation here.

A simple consequence is that if we draw $x_i(0)$ from a distribution supported on χ_i , then all initial configurations will be “typical”, and hence, at large times, they all result in $\mathbb{P}_{\text{qu}}[T, t]$. Consequently, within this initialization protocol, the quenched and the annealed probability distributions are the same.

IV. THE LARGE DEVIATION FUNCTIONS

In the previous section we have described the behavior of the occupation time close to its typical value in both annealed and quenched cases for general steplike initial conditions. In this section we focus on the uncorrelated uniform initial condition and study the tails of the probability distributions (7) and (8).

The mean and the variances we have computed suggest that at large times probability distributions admit the following forms

$$\mathbb{P}_{\text{an}}[T, t] \simeq \exp \left[-\bar{\rho}\sqrt{4Dt} \Phi_{\text{an}}(\tau) \right], \quad (91)$$

$$\mathbb{P}_{\text{qu}}[T, t] \simeq \exp \left[-\bar{\rho}\sqrt{4Dt} \Phi_{\text{qu}}(\tau) \right], \quad (92)$$

with

$$\tau \equiv \frac{T}{t^{3/2}} \frac{1}{\bar{\rho}\sqrt{4D}}. \quad (93)$$

In what follows we compute rate functions $\Phi_{\text{an}}(\tau)$ and $\Phi_{\text{qu}}(\tau)$ along with their asymptotic expansions.

A. Annealed large deviation function

As we have shown in (85) annealed probability distribution depends on the initial condition, and this dependence does not vanish with time. Clearly such dependence remains on the level of the rate function $\Phi_{\text{an}}(\tau)$ and has significant impact on the tails of the probability distribution. Thus we focus on the uncorrelated uniform initial condition. In this case

$$\overline{\langle e^{-pT} \rangle}_{\mathbf{x}} = \left[\int_{-L}^0 \frac{dx}{L} \langle e^{-pT} \rangle_x \right]^N. \quad (94)$$

The exact form of $\langle e^{-pT} \rangle_x$ is given by (41) and consists of two terms. Integral of the first term can be computed exactly and its large L behavior reads

$$\int_{-L}^0 \frac{dx}{L} \operatorname{erf} \left[\frac{|x|}{\sqrt{4Dt}} \right] \underset{L \rightarrow \infty}{\simeq} 1 - \frac{1}{L} \sqrt{\frac{4Dt}{\pi}}. \quad (95)$$

To determine the behavior of the second term we first integrate with respect to x , then take the limit $L \rightarrow \infty$

$$\begin{aligned} & \frac{1}{\pi} \int_{-L}^0 \frac{dx}{L} \int_0^1 d\xi \frac{e^{-pt\xi}}{\sqrt{\xi(1-\xi)}} \exp \left[-\frac{x^2}{4Dt} \frac{1}{(1-\xi)} \right] \\ &= \frac{1}{L} \sqrt{\frac{tD}{\pi}} \int_0^1 d\xi \frac{e^{-pt\xi}}{\sqrt{\xi}} \operatorname{erf} \left[\frac{L}{\sqrt{4Dt(1-\xi)}} \right] \\ & \underset{L \rightarrow \infty}{\simeq} \frac{1}{L} \sqrt{\frac{tD}{\pi}} \int_0^1 d\xi \frac{e^{-pt\xi}}{\sqrt{\xi}} \\ &= \frac{1}{L} \sqrt{\frac{D}{p}} \operatorname{erf}(\sqrt{pt}) \end{aligned} \quad (96)$$

Combining (96) with (95) we obtain for (94)

$$\overline{\langle e^{-pT} \rangle}_{\mathbf{x}} \underset{L \rightarrow \infty}{\simeq} \left[1 - \frac{1}{L} \sqrt{\frac{4Dt}{\pi}} + \frac{1}{L} \sqrt{\frac{D}{p}} \operatorname{erf}(\sqrt{pt}) \right]^N \quad (97)$$

hence in the thermodynamic limit $N, L \rightarrow \infty$ with the fixed ratio $\bar{\rho} = N/L$ we have

$$\overline{\langle e^{-pT} \rangle}_{\mathbf{x}} \underset{L, N \rightarrow \infty}{\simeq} \exp \left[-\bar{\rho} \sqrt{4Dt} \phi_{\text{an}}(pt) \right] \quad (98)$$

where

$$\phi_{\text{an}}(q) = \frac{1}{\sqrt{\pi}} - \frac{1}{\sqrt{4q}} \operatorname{erf}(\sqrt{q}). \quad (99)$$

In principle to find the annealed probability distribution $\mathbb{P}_{\text{an}}[T, t]$ we need to invert double Laplace transform

$$\int_{0^-}^{\infty} dT e^{-pT} \mathbb{P}_{\text{an}}[T, t] = \exp \left[-\bar{\rho} \sqrt{4Dt} \phi_{\text{an}}(pt) \right]. \quad (100)$$

However, since we are interested in the large time behavior, we can instead substitute ansatz (91) into (100). Then after rescaling of the variables we get

$$\int_{0^-}^{\infty} d\tau e^{-\bar{\rho} \sqrt{4Dt} (q\tau + \Phi_{\text{an}}(q))} = e^{-\bar{\rho} \sqrt{4Dt} \phi_{\text{an}}(q)}, \quad (101)$$

where

$$q = pt, \quad \tau = \frac{T}{t^{3/2}} \frac{1}{\bar{\rho} \sqrt{4D}}. \quad (102)$$

Large time limit corresponds to the saddle point approximation of the integral in (101). By comparing exponents we find that

$$\min_{\tau} (q\tau + \Phi_{\text{an}}(\tau)) = \phi_{\text{an}}(q). \quad (103)$$

Inverting Legendre transform (103) we obtain

$$\Phi_{\text{an}}(\tau) = \max_q (-q\tau + \phi_{\text{an}}(q)). \quad (104)$$

Expression (104) together with (99) provides us with the parametric representation of the annealed large deviation function $\Phi_{\text{an}}(\tau)$. It is a concave function with the minimum at some point τ_{typ} . Due to (58) we indeed expect $\tau_{\text{typ}} = \frac{1}{3\sqrt{\pi}}$. Furthermore, by analyzing $\phi_{\text{an}}(q)$ at $q \rightarrow 0$, $q \rightarrow \infty$ and $q \rightarrow -\infty$ we can extract asymptotic behavior of $\Phi_{\text{an}}(\tau)$ for $\tau \rightarrow \tau_{\text{typ}}$, $\tau \rightarrow 0$ and $\tau \rightarrow \infty$ respectively. Below we provide the computation eventually arriving at (23).

1. Typical fluctuations

Typical fluctuations of the occupation time are governed by the behavior of the $\phi_{\text{an}}(q)$ close to $q = 0$. By expanding (99) up to the second order in q we find

$$\phi_{\text{an}}(q) \simeq \frac{1}{\sqrt{\pi}} \left(\frac{1}{3}q - \frac{1}{10}q^2 \right), \quad q \rightarrow 0 \quad (105)$$

and hence

$$\Phi_{\text{an}}(\tau) \simeq \max_q \left(-q\tau + \frac{1}{\sqrt{\pi}} \left(\frac{1}{3}q - \frac{1}{10}q^2 \right) \right). \quad (106)$$

This is a quadratic function and we easily find that

$$\Phi_{\text{an}}(\tau) \simeq \frac{5}{2} \sqrt{\pi} \left(\tau - \frac{1}{3\sqrt{\pi}} \right)^2, \quad \tau \rightarrow \tau_{\text{typ}} = \frac{1}{3\sqrt{\pi}} \quad (107)$$

which implies

$$\mathbb{P}_{\text{an}}[T, t] \simeq \exp \left[-\frac{1}{2} \left(\frac{T - T_{\text{typ}}}{\sigma_{\text{an}}} \right)^2 \right], \quad T \rightarrow T_{\text{typ}} \quad (108)$$

with

$$T_{\text{typ}} = \frac{2}{3} \sqrt{\frac{D}{\pi}} \bar{\rho} t^{3/2}, \quad \sigma_{\text{an}}^2 = \frac{2}{5} \sqrt{\frac{D}{\pi}} \bar{\rho} t^{5/2}. \quad (109)$$

In other words, large deviation function gives us exactly the same results as we have obtained in the previous section by different means (recall (58) and (89)).

2. Atypical fluctuations $T \ll T_{\text{typ}}$

Atypically small fluctuations are governed by large q behavior of the $\phi_{\text{an}}(q)$. Expanding (99) in series as $q \rightarrow \infty$ we get

$$\phi_{\text{an}}(q) \simeq \frac{1}{\sqrt{\pi}} - \frac{1}{\sqrt{4q}}, \quad q \rightarrow \infty. \quad (110)$$

Therefore

$$\Phi_{\text{an}}(\tau) \simeq \max_q \left(-q\tau + \frac{1}{\sqrt{\pi}} - \frac{1}{\sqrt{4q}} \right). \quad (111)$$

Maximizing this function we arrive at

$$\Phi_{\text{an}}(\tau) \simeq \frac{1}{\sqrt{\pi}} - \frac{3}{2} \left(\frac{\tau}{2} \right)^{1/3}, \quad \tau \rightarrow 0. \quad (112)$$

3. Atypical fluctuations $T \gg T_{\text{typ}}$

To study atypically large fluctuations we need to expand $\phi_{\text{an}}(q)$ as $q \rightarrow -\infty$. The subtlety here lies in the square root, namely we need to perform an analytical continuation of the $\operatorname{erf}(z)$ as

$$\phi_{\text{an}}(q) = \frac{1}{\sqrt{\pi}} + \frac{i \operatorname{erf}(i\sqrt{|q|})}{\sqrt{4|q|}}, \quad q < 0, \quad (113)$$

and using the expansion

$$i \operatorname{erf}(i\sqrt{|q|}) \simeq -\frac{e^{|q|}}{\sqrt{\pi|q|}}, \quad q \rightarrow -\infty \quad (114)$$

we arrive at

$$\Phi_{\text{an}}(\tau) \simeq \max_q \left(|q|\tau + \frac{1}{\sqrt{\pi}} - \frac{1}{\sqrt{\pi}} \frac{e^{|q|}}{2|q|} \right). \quad (115)$$

Taking the derivative of the expression in (115) we find that its maximum is reached at $q = q^*$ satisfying

$$\tau - \frac{e^{|q^*|}}{2\sqrt{\pi}|q^*|} = 0 \quad (116)$$

This is a well-known transcendent equation, and its solution is expressed in terms of the Lambert W -function [50]. For $\tau > \frac{e}{2\sqrt{\pi}}$ there are two roots of (116), but since we are looking at $\tau \rightarrow \infty$ we should choose the solution corresponding to the larger τ . It is given by the lower branch of the Lambert W -function

$$q^* = W_{-1} \left(-\frac{1}{2\tau\sqrt{\pi}} \right). \quad (117)$$

Utilizing the asymptotic expansion of $W_{-1}(z)$

$$W_{-1}(-z) \simeq \log z - \log[-\log z], \quad z \rightarrow 0 \quad (118)$$

we find that in the leading order

$$|q^*| \simeq \log[2\tau\sqrt{\pi}] + \log \log[2\tau\sqrt{\pi}], \quad \tau \rightarrow \infty. \quad (119)$$

Substituting (119) into (115) we get the asymptotic behavior of the large deviation function

$$\Phi_{\text{an}}(\tau) \simeq \tau \left(\mu(\tau) \log[2\tau\sqrt{\pi}] - \frac{1}{\mu(\tau)} \right), \quad \tau \rightarrow \infty. \quad (120)$$

where

$$\mu(\tau) = 1 + \frac{\log \log[2\tau\sqrt{\pi}]}{\log[2\tau\sqrt{\pi}]}. \quad (121)$$

B. Quenched large deviation function

Now we proceed to the quenched probability distribution (8). As we have shown in (65) its Laplace transform reads

$$\int_0^t dT e^{-pT} \mathbb{P}_{\text{qu}}[T, t] = \exp \left[\bar{\rho} \int_0^\infty dy \log \langle e^{-pT} \rangle_y \right]. \quad (122)$$

Using the explicit form (41) of $\langle e^{-pT} \rangle_y$ we find that the quenched probability distribution is given by

$$\int_0^t dT e^{-pT} \mathbb{P}_{\text{qu}}[T, t] = \exp \left[-\bar{\rho} \sqrt{4Dt} \phi_{\text{qu}}(pt) \right] \quad (123)$$

where

$$\phi_{\text{qu}}(q) = - \int_0^\infty dy \log \left[\text{erf}(y) + \frac{1}{\pi} \int_0^1 d\xi \frac{e^{-q\xi - \frac{y^2}{1-\xi}}}{\sqrt{\xi(1-\xi)}} \right]. \quad (124)$$

Analogously to the annealed case we find that in the saddle-point approximation

$$\mathbb{P}_{\text{qu}}[T, t] \simeq \exp \left[-\bar{\rho} \sqrt{4Dt} \Phi_{\text{qu}}(\tau) \right], \quad \tau = \frac{T}{t^{3/2}} \frac{1}{\bar{\rho} \sqrt{4D}}, \quad (125)$$

where the large deviation function $\Phi_{\text{qu}}(\tau)$ is given by an inverse Legendre transform

$$\Phi_{\text{qu}}(\tau) = \max_q (-q\tau + \phi_{\text{qu}}(q)). \quad (126)$$

Equations (126) and (124) give the parametric representation of $\Phi_{\text{qu}}(\tau)$. Let us now study its asymptotic behavior and derive (29).

1. Typical fluctuations

In order to obtain fluctuations of the occupation time close to the typical value we need to study the behavior of $\phi_{\text{qu}}(q)$ as $q \rightarrow 0$. By first expanding the integrals in (124) in series with respect to q and then using the representation of the moments in terms of confluent hypergeometric function (44) as in (43), after technical yet straightforward computation we arrive at

$$\phi_{\text{qu}}(q) \simeq \frac{1}{3\sqrt{\pi}} q - \frac{4}{15} \frac{\sqrt{2}-1}{\sqrt{\pi}} q^2, \quad q \rightarrow 0. \quad (127)$$

Therefore in accordance with (126) we have

$$\Phi_{\text{qu}}(\tau) \simeq \max_q \left(-q\tau + \frac{1}{3\sqrt{\pi}} q - \frac{4}{15} \frac{\sqrt{2}-1}{\sqrt{\pi}} q^2 \right). \quad (128)$$

Maximizing this quadratic function yields

$$\Phi_{\text{qu}}(\tau) \simeq \frac{1}{2} \frac{15\sqrt{\pi}}{4(\sqrt{2}-1)} \left(\tau - \frac{1}{3\sqrt{\pi}} \right)^2, \quad \tau \rightarrow \tau_{\text{typ}} = \frac{1}{3\sqrt{\pi}}. \quad (129)$$

Expression (129) implies that close to the typical value, the quenched probability distribution behaves as

$$\mathbb{P}_{\text{qu}}[T, t] \simeq \exp \left[-\frac{1}{2} \left(\frac{T - T_{\text{typ}}}{\sigma_{\text{qu}}} \right)^2 \right], \quad T \rightarrow T_{\text{typ}} \quad (130)$$

where

$$T_{\text{typ}} = \frac{2}{3} \sqrt{\frac{D}{\pi}} \bar{\rho} t^{3/2}, \quad \sigma_{\text{qu}}^2 = \frac{8(\sqrt{2}-1)}{15} \sqrt{\frac{D}{\pi}} \bar{\rho} t^{5/2}. \quad (131)$$

This is exactly the behavior anticipated in (58) and (62).

2. Atypical fluctuations $T \ll T_{\text{typ}}$

Atypically small fluctuations can be extracted from the $q \rightarrow \infty$ expansion of $\phi_{\text{qu}}(q)$. First we note, that in (124) the main contribution to the integral over ξ comes from values of ξ close to zero, therefore

$$\int_0^1 d\xi \frac{e^{-q\xi - \frac{y^2}{1-\xi}}}{\sqrt{\xi(1-\xi)}} \simeq e^{-y^2} \int_0^1 d\xi \frac{e^{-q\xi}}{\sqrt{\xi}}, \quad q \rightarrow \infty. \quad (132)$$

Computing this integral yields

$$\int_0^1 d\xi \frac{e^{-q\xi}}{\sqrt{\xi}} = \frac{\sqrt{\pi} \operatorname{erf}(\sqrt{q})}{\sqrt{q}} \simeq \sqrt{\frac{\pi}{q}}, \quad q \rightarrow \infty. \quad (133)$$

Substituting (133) and (132) into (124) we arrive at

$$\phi_{\text{qu}}(q) \simeq - \int_0^\infty dy \log \left[\operatorname{erf}(y) + e^{-y^2} \frac{1}{\sqrt{\pi q}} \right], \quad q \rightarrow \infty. \quad (134)$$

To proceed further we use a trick. Namely, we take a derivative of $\phi_{\text{qu}}(q)$

$$\frac{\partial}{\partial q} \phi_{\text{qu}}(q) = \frac{1}{2q^{3/2}} \int_0^\infty dy \frac{1}{\frac{1}{\sqrt{q}} + e^{y^2} \sqrt{\pi} \operatorname{erf}(y)}. \quad (135)$$

and note, that the integral (135) diverges as $q \rightarrow \infty$. To determine the large q behavior of $\phi_{\text{qu}}(q)$, it is sufficient to find the divergent part of (135) and integrate it back. This can be done by rewriting the integral in (135) as

$$\begin{aligned} & \int_0^\infty dy \frac{1}{\frac{1}{\sqrt{q}} + e^{y^2} \sqrt{\pi} \operatorname{erf}(y)} \\ &= \int_0^1 dy \left(\frac{1}{\frac{1}{\sqrt{q}} + e^{y^2} \sqrt{\pi} \operatorname{erf}(y)} - \frac{1}{\frac{1}{\sqrt{q}} + 2y} \right) \\ &+ \int_1^\infty dy \frac{1}{\frac{1}{\sqrt{q}} + e^{y^2} \sqrt{\pi} \operatorname{erf}(y)} + \int_0^1 \frac{1}{\frac{1}{\sqrt{q}} + 2y} dy. \end{aligned} \quad (136)$$

In (136) first two integrals converge, computing them we get

$$\begin{aligned} & \int_0^\infty dy \frac{1}{\frac{1}{\sqrt{q}} + e^{y^2} \sqrt{\pi} \operatorname{erf}(y)} \\ & \simeq \frac{1}{4} \log \frac{\pi}{4} + \int_0^1 \frac{1}{\frac{1}{\sqrt{q}} + 2y} dy \end{aligned} \quad (137)$$

the remaining integral diverges logarithmically, hence

$$\frac{\partial}{\partial q} \phi_{\text{qu}}(q) \simeq \frac{1}{8q^{3/2}} \log \pi q, \quad q \rightarrow \infty. \quad (138)$$

Integrating (138) back gives us

$$\phi_{\text{qu}}(q) = \phi_\infty - \frac{2 + \log \pi q}{4\sqrt{q}}, \quad (139)$$

where the constant of integration is restored by taking the limit $q \rightarrow \infty$ in (134)

$$\phi_\infty = - \int_0^\infty \log [\operatorname{erf}(y)] dy \approx 1.03. \quad (140)$$

The only thing left is to invert the Legendre transform

$$\Phi_{\text{qu}}(\tau) \simeq \max_q \left(-q\tau + \phi_\infty - \frac{2 + \log \pi q}{4\sqrt{q}} \right) \quad (141)$$

Maximum of this expression is reached at q^* , a root of

$$-\tau + \frac{1}{8q^{3/2}} \log \pi q^* = 0. \quad (142)$$

After a change of variables $q = \frac{1}{\pi} \exp[-\frac{2}{3}u]$ equation (142) transforms into

$$e^u + \frac{12\tau}{u \pi^{3/2}} = 0. \quad (143)$$

We have already solved this equation in (116) and its solution is given in terms of the lower branch of the Lambert W -function as

$$q^* = \frac{1}{\pi} \exp \left[-\frac{2}{3} W_{-1} \left(-\frac{12\tau}{\pi^{3/2}} \right) \right], \quad \tau \rightarrow 0. \quad (144)$$

Using the asymptotic expansion for $W_{-1}(z)$ as in (118) we find that in the leading order

$$q^* \simeq \left(\frac{1}{12\tau} \log \frac{\pi^{3/2}}{12\tau} \right)^{2/3}, \quad \tau \rightarrow 0 \quad (145)$$

and hence

$$\Phi_{\text{qu}}(\tau) \simeq \phi_\infty - \frac{1 + \frac{1}{2} \log \nu + \frac{1}{3} \log \log \nu}{\frac{2}{\sqrt{\pi}} (\nu \log \nu)^{1/3}}, \quad \tau \rightarrow 0 \quad (146)$$

where

$$\nu = \frac{\pi^{3/2}}{12\tau}. \quad (147)$$

3. Atypical fluctuations $T \gg T_{\text{typ}}$

Atypically large fluctuations correspond to $q \rightarrow -\infty$ expansion of $\phi_{\text{qu}}(q)$. To obtain this expansion we perform the change of variables $y \mapsto y\sqrt{|q|}$ and $\xi \mapsto 1 - \xi$ in (124) arriving at

$$\begin{aligned} \phi_{\text{qu}}(q) &= -\sqrt{|q|} \int_0^\infty dy \\ & \log \left[\operatorname{erf} \left(y\sqrt{|q|} \right) + \frac{1}{\pi} \int_0^1 d\xi \frac{e^{-|q| \left(\frac{y^2}{\xi} + \xi - 1 \right)}}{\sqrt{\xi(1-\xi)}} \right]. \end{aligned} \quad (148)$$

The integral over ξ can be evaluated in the saddle-point approximation yielding

$$\frac{1}{\pi} \int_0^1 d\xi \frac{e^{-|q| \left(\frac{y^2}{\xi} + \xi - 1 \right)}}{\sqrt{\xi(1-\xi)}} \simeq \frac{e^{-|q|(2y-1)}}{\sqrt{\pi|q|(1-y)}}, \quad q \rightarrow -\infty, \quad (149)$$

hence we have

$$\phi_{\text{qu}}(q) \simeq -\sqrt{|q|} \int_0^\infty dy \log \left[1 + \frac{e^{-|q|(2y-1)}}{\sqrt{\pi|q|(1-y)}} \right]. \quad (150)$$

Integrating by parts we get

$$\phi_{\text{qu}}(q) \simeq -\sqrt{|q|} \int_0^1 dy \frac{2y|q|}{1 + \sqrt{\pi|q|} e^{-|q|(1-2y)}}. \quad (151)$$

This is a complete Fermi-Dirac integral which can be evaluated in terms of the polylogarithm function

$$\phi_{\text{qu}}(q) \simeq \frac{1}{2\sqrt{|q|}} \text{Li}_2 \left(-\frac{e^{|q|}}{\sqrt{\pi|q|}} \right), \quad q \rightarrow -\infty \quad (152)$$

and using the expansion

$$\text{Li}_2(-z) \simeq -\frac{1}{2} \log^2(z), \quad z \rightarrow \infty \quad (153)$$

we finally find that

$$\phi_{\text{qu}}(q) \simeq -\frac{1}{4}|q|^{3/2}, \quad q \rightarrow -\infty. \quad (154)$$

Thus the large deviation function is given by

$$\Phi_{\text{qu}}(\tau) \simeq \max_q \left(-q\tau - \frac{1}{4}(-q)^{3/2} \right) \quad (155)$$

and hence

$$\Phi_{\text{qu}}(\tau) \simeq \left(\frac{4}{3} \tau \right)^3, \quad \tau \rightarrow \infty. \quad (156)$$

V. NUMERICAL SIMULATIONS

To support our analytical calculations we perform numerical simulations. Since there is no interaction, the total occupation time is nothing but a sum of occupation times for individual particles. Therefore, in order to explore probability distributions (7) and (8) we can sample N single particle occupation times from (37) while choosing appropriate initial conditions. However in this process we encounter two problems.

The first problem involves effectively sampling from (37). The second problem is more intricate, as it entails capturing samples with atypical values of the occupation time. Since the probability of getting such values is very small, we cannot reach the tails of the distribution when sampling from (37). Fortunately, both problems can be resolved. To address the first problem, we introduce an additional variable corresponding to the first hitting time and sample occupation time in two steps. The second problem, although more subtle, is well known and in many situations can be resolved by Importance Sampling Monte-Carlo [3, 51–55]. Here we shall utilize this approach as well.

A. Sampling strategy

First we address the problem of sampling from the probability distribution of the single particle occupation time

$\mathbb{P}[T, t, |x]$. To do this we rewrite (37) as

$$\begin{aligned} \mathbb{P}[T, t, |x] &= \int_t^\infty d\omega \delta(T) \mathbb{F}[\omega | x] \\ &+ \int_0^t d\omega \mathbb{P}[T, t - \omega | x = 0] \mathbb{F}[\omega | x] \end{aligned} \quad (157)$$

where

$$\mathbb{F}[\omega | x] = \frac{|x|}{\sqrt{4\pi D\omega^3}} \exp \left[-\frac{x^2}{4D\omega} \right]. \quad (158)$$

Function $\mathbb{F}[\omega | x]$ in (158) is nothing but a probability distribution of the first passage time [56], i.e. ω is the time at which Brownian particle reaches the origin for the first time given the initial position x . The factor $\mathbb{P}[T, t - \omega | x = 0]$ according to (37) is

$$\mathbb{P}[T, t - \omega | x = 0] = \frac{1}{\pi} \frac{1}{\sqrt{T(t - \omega - T)}} \mathbb{1}_{[0, t - \omega]}(T). \quad (159)$$

In (159) we added an indicator function, to emphasize, that the distribution is supported on the segment $[0, t - \omega]$.

The sampling procedure for the occupation time of an individual particle is now as follows: first we sample ω from $\mathbb{F}[\omega | x]$ given by (158); if $\omega \geq t$, i.e. the particle does not reach the origin up to the observation time, then occupation time is zero (it corresponds to the first term in (157)), otherwise we sample occupation time T from $\mathbb{P}[T, t - \omega | x = 0]$ in (159). Since both (158) and (159) are relatively simple, we sample from them directly. This way, we can effectively draw occupation time for a single particle with fixed initial position.

Now we proceed to the problem of exploring the tails of the probability distribution. To address it, we utilize Importance Sampling Monte-Carlo technique. Let us briefly recall its basics.

Consider a random variable z with probability distribution $\mathbb{P}[z]$ and suppose that our goal is to compute an average value of some observable $O(z)$

$$\langle O(z) \rangle = \int dz O(z) \mathbb{P}[z] \quad (160)$$

The usual Monte-Carlo strategy is to get n samples z_i from $\mathbb{P}[z]$ and estimate an average by

$$\langle O(z) \rangle \approx \frac{1}{n} \sum_i O(z_i), \quad z_i \leftarrow \mathbb{P}[z]. \quad (161)$$

To study the probability distribution itself we can choose the observable to be an indicator function

$$O(z) = \mathbb{1}_{[z_1; z_2]}(z) \equiv \begin{cases} 1, & z \in [z_1, z_2], \\ 0, & z \notin [z_1, z_2]. \end{cases} \quad (162)$$

The average value of the indicator function is nothing but the probability that z falls into the interval $[z_1, z_2]$

$$\langle \mathbb{1}_{[z_1; z_2]}(z) \rangle = \mathbb{P}[z_1 \leq z \leq z_2]. \quad (163)$$

By choosing sufficiently small interval $[z_0, z_0 + dz]$ we get the probability distribution itself

$$\langle \mathbb{1}_{[z_0, z_0 + dz]}(z) \rangle = \mathbb{P}[z_0] dz. \quad (164)$$

If we are interested in the tails of the probability distribution where $\mathbb{P}[z]$ is usually very small, then the above procedure is ill-suited. Indeed, the smaller $\mathbb{P}[z_0]$ the rarer we get values laying in $[z_0, z_0 + dz]$. Of course, in the limit $n \rightarrow \infty$ approximation (161) becomes exact, however in practice it may require unreasonably many samples.

To overcome this problem we rewrite (160) as

$$\langle O(z) \rangle = \int dz \left(O(z) \frac{\mathbb{P}[z]}{\mathbb{Q}[z]} \right) \mathbb{Q}[z] \quad (165)$$

where $\mathbb{Q}[z]$ is some, for the moment arbitrary, probability distribution. Comparing (165) with (160) we see that instead of (161) we can use

$$\langle O(z) \rangle \approx \frac{1}{n} \sum_i O(z_i) \frac{\mathbb{P}[z_i]}{\mathbb{Q}[z_i]}, \quad z_i \leftarrow \mathbb{Q}[z]. \quad (166)$$

where z_i are drawn from $\mathbb{Q}[z]$ and not from $\mathbb{P}[z]$ as in (161).

Formally (161) and (166) are indeed equivalent. But by an appropriate choice of $\mathbb{Q}[z]$ we can drastically decrease the number of samples required for an approximation to be accurate enough.

Now we return to the problem of a Brownian motion. To implement Importance Sampling strategy, we introduce an exponential tilt in (37), and sample occupation time from

$$\mathbb{Q}[T, t | x] = \frac{1}{Z(\beta, t | x)} e^{-\beta \frac{T}{t}} \mathbb{P}[T, t | x] \quad (167)$$

where the normalization $Z(\beta, t | x)$ is

$$Z(\beta, t | x) = \int_0^t dT e^{-\beta \frac{T}{t}} \mathbb{P}[T, t | x]. \quad (168)$$

By varying the parameter β in (167) we can bias the trajectories. Namely, positive (negative) values of β bias the trajectories with small (large) occupation time. To get the sample of the occupation time from the tilted distribution (167) we use Metropolis algorithm [57], i.e. sample new value of occupation time \tilde{T} from $\mathbb{P}[T, t | x]$ and accept the “move” with probability $\min\left(1, e^{-\beta \frac{\tilde{T}-T}{t}}\right)$.

B. Probability distributions

1. Quenched distribution

The quenched probability distribution corresponds to the typical configuration of particles. One of the ways to realize a typical configuration is to take equidistantly distributed particles. Therefore to mimic the quenched probability distribution we consider frozen initial condition (example (a) in Fig. 5)

$$x_i \equiv x_i(0) = -\frac{i - \frac{1}{2}}{\bar{\rho}}, \quad i = 1, \dots, N. \quad (169)$$

The quenched probability distribution can then be approximated as

$$\mathbb{P}_{\text{qu}}[T, t] dT \approx \frac{1}{n} \sum_i \mathbb{1}_{[T, T+dT]} \left(\sum_{j=1}^N T_j \right) \prod_{j=1}^N \frac{\mathbb{P}[T, t | x_j]}{\mathbb{Q}[T, t | x_j]} \quad (170)$$

with x_j given by (169) and T_j sampled from the tilted distribution $\mathbb{Q}[T, t | x_i]$ as in (167)

$$T_j \leftarrow \mathbb{Q}[T, t | x_j]. \quad (171)$$

To get the sample of N single particle occupation times, we use Metropolis algorithm. At each step we pick some fraction $r < N$ of single particle occupation times T_j and resample them. The value of r is chosen in such a way that approximately half of proposed Metropolis steps are accepted.

In numerical simulation we use $D = 0.5$, $N = 10^4$, $L = 10^4$ ($\bar{\rho} = 1$) and $t = 1000$. For each value of β we produce 10^6 configurations (that is 10^{10} samples of a single particle occupation times). To compare simulations with the analytical results we compute $Z(\beta, t | x_j)$ in (168) and the normalization constant in (92) numerically. Resulting plots are given in Fig 6.

2. Annealed distribution

The only difference with respect to the quenched case is that now initial coordinates are not fixed but drawn from the uniform distribution on the segment $[-L; 0]$. Hence we approximate the probability distribution as

$$\mathbb{P}_{\text{an}}[T, t] dT \approx \frac{1}{n} \sum_i \mathbb{1}_{[T, T+dT]} \left(\sum_{j=1}^N T_j \right) \prod_{j=1}^N \frac{\mathbb{P}[T_j, t; x_j]}{\mathbb{Q}[T_j, t; x_j]}. \quad (172)$$

where we sample (T_j, x_j) from

$$(x_j, T_j) \leftarrow \mathbb{Q}[T, t; x_j]. \quad (173)$$

and $\mathbb{P}[T, t; x]$ and $\mathbb{Q}[T, t; x]$ are joint distributions of the occupation time and initial coordinate, given by

$$\mathbb{P}[T, t; x] = \frac{1}{L} \mathbb{P}[T, t | x], \quad (174)$$

$$\mathbb{Q}[T, t; x] = \frac{1}{Z(\beta, t)} e^{-\beta \frac{T}{t}} \mathbb{P}[T, t; x]. \quad (175)$$

The normalization in (175) is

$$Z(\beta, t) = \int_{-L}^0 dx \int_0^t dT e^{-\beta \frac{T}{t}} \mathbb{P}[T, t; x]. \quad (176)$$

Note that constants in (175) and (167) are related via

$$Z(\beta, t) = \int_{-L}^0 \frac{dx}{L} Z(\beta, t | x). \quad (177)$$

The sampling strategy is the same as in the quenched case, and the only difference is that we instead of using (169) we sample x from the uniform distribution.

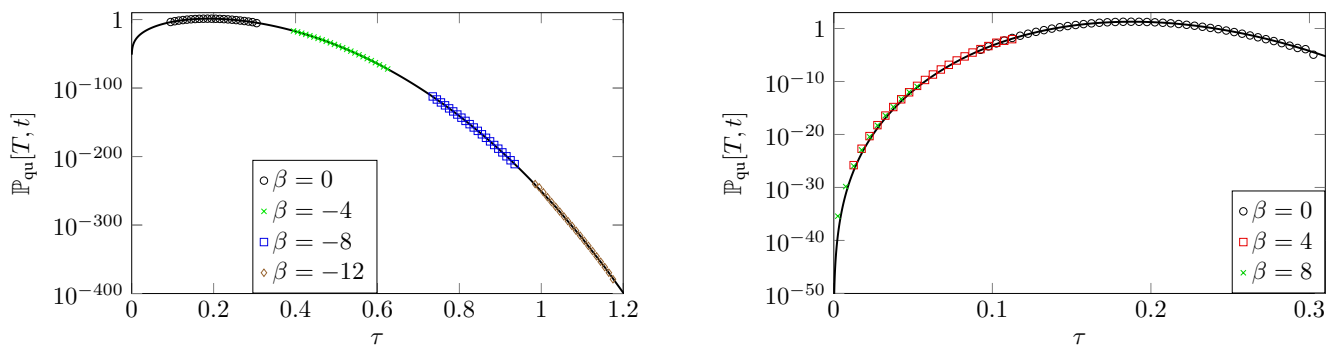


Figure 6. The quenched probability distribution obtained from (19), (27) and (28) (solid lines). Results of the simulations for the negative (positive) values of tilt β in (167) are shown in the left (right) plane. Different shapes correspond to the different values of the tilt β .

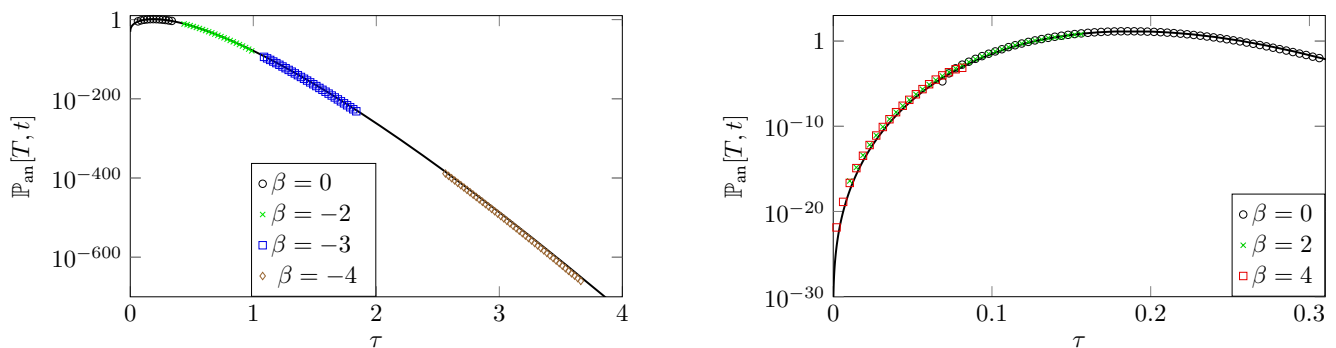


Figure 7. The annealed probability distribution obtained from (18), (21) and (22) (solid lines). Results of the simulations for the negative (positive) values of tilt β in (175) are shown in the left (right) plane. Different shapes correspond to the different values of the tilt β .

In numerical simulation we use $D = 0.5$, $N = 10^4$, $L = 10^4$ ($\bar{\rho} = 1$) and $t = 1000$. For each value of β we produce 10^6 configurations (that is 10^{10} samples of a single particle occupation times). To compare numerical results with the analytical we compute $Z(\beta, t)$ in (176) and the normalization constant in (91) numerically. Resulting plots are given in Fig 7.

As a side comment, let us mention, that on the contrary to [3] we do not directly bias the distribution of the initial coordinates of particles.

C. Impact of the initial conditions

One of the advantages of the Metropolis algorithm is that it tells us which trajectories contribute to the atypical values of the occupation time.

In the quenched case, the initial coordinates of particles are fixed, and atypically large values in principle can be reached via two mechanisms. First option is that a lot of particles contribute slightly more than they typically would, but due to their numbers, total occupation time is atypically large. The second option is that the main contribution comes from a small number of particles which have extremely large values of the occupation time. By plotting average values of the

single particle occupation times T_j (Fig 9) we see that the latter mechanism is in work here. For the atypically small values of the occupation time we see a similar picture. In other words both tails of the quenched probability distributions are governed by just a handful of particles.

As a consistency check, recall that the mean square displacement of a Brownian particle is $\sqrt{\langle \Delta x^2 \rangle} = \sqrt{2Dt}$ which in our simulation is $\sqrt{\langle \Delta x^2 \rangle} = 100$. Therefore we expect approximately 100 out of 10000 particles to contribute to the typical values of the occupation time. From Fig. 9 we see that this is exactly the case.

On the contrary to the quenched distribution, the annealed one takes into account atypical initial conditions. As we argued in Sec II B, this leads to the higher probabilities of both atypically large and atypically small values of the occupation times. Indeed, configurations with particles initialized close to (far from) the origin should lead to large (small) values of the occupation time. This can be observed by plotting average initial density of particles for different values of the tilt β (see Fig. 8, left). In addition, by plotting average value of the occupation time as a function of the initial position (see Fig. 8, right), we see that, as in the quenched case, atypical values of the occupation time are governed by a small faction of particles located close to the origin. This clearly shows that both

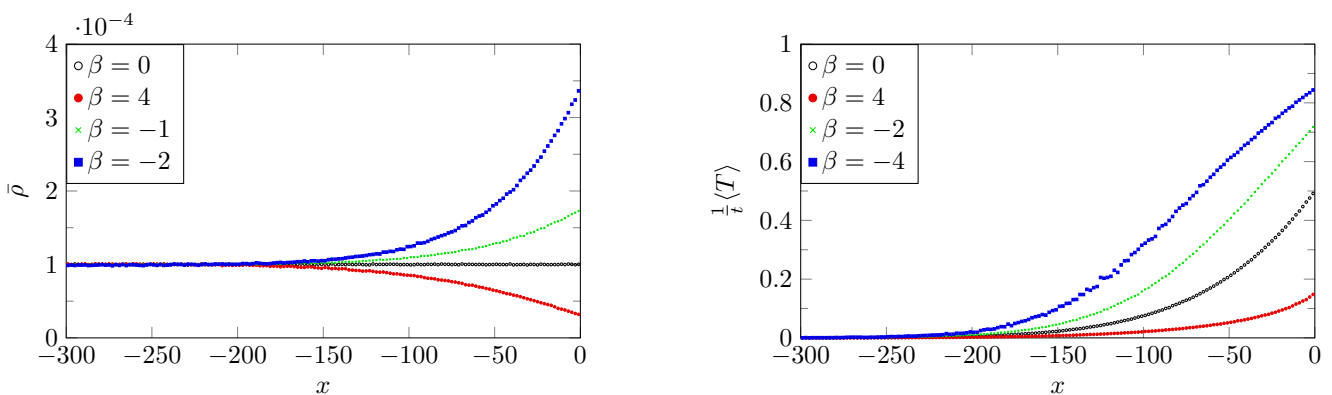


Figure 8. The annealed case: Average initial density profile (left) and average value of the single particle occupation time as a function of its initial position (right). Different shapes correspond to the different values of the tilt β . From the left plane it is clear that atypically large values of the occupation time correspond to the initial conditions with particles localized close to the origin whereas atypically small values of the occupation time correspond to the configuration with the vicinity of the origin being depopulated. Right plane shows that, as in the quenched case, atypical values of the occupation time are due the particles initially located close to the origin.

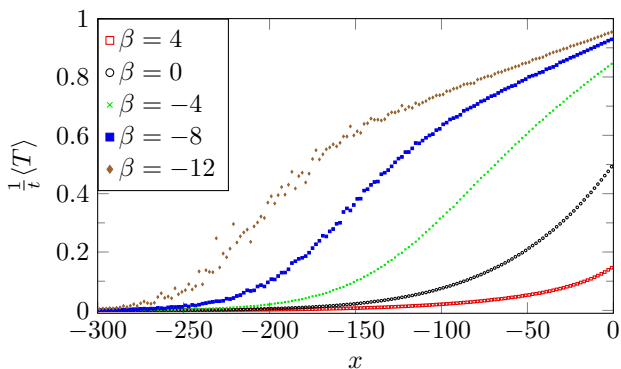


Figure 9. The quenched case: Average value of the single particle occupation time as a function of its initial position. Different shapes correspond to the different values of the tilt β . Atypically small and atypically large values of the total occupation time originate from a bunch of particles close to the origin.

randomness in the initial configuration and stochasticity of trajectories contribute to the atypical values of the occupation time in the annealed case.

VI. CONCLUSION

We have considered a system of noninteracting Brownian particles on the line with steplike initial conditions focusing on a particular observable, occupation time on the half line. In this paper we have derived several exact asymptotic results that are summarized below.

We have computed the mean and the variance of the occupation time on the half-line for the general steplike initial condition. We have shown that the dependence of the variance on the initial condition is encoded in the single

static quantity known as generalized compressibility (Fano factor). For the uncorrelated uniform initial condition we have found the large deviation forms of the quenched and the annealed probability distributions. By computing the corresponding large deviation functions we have described the tails of these probability distributions. Two resulting distributions are very different. As a verification of the theoretical results we performed numerical simulations with Importance Sampling Monte-Carlo.

We emphasize that, despite the similarity in the methods, the results for the occupation time presented in this paper could have not been predicted based on those obtained by the authors in [3] for the local time. However, given the similarity in the analysis, it is natural to inquire whether the same methods can be extended further to study other functionals, such as the area under a Brownian excursion, for example.

There are several natural directions in which it would be interesting to generalize our results. First and foremost we can consider more general, though still noninteracting systems. This includes introducing external potential or stochastic resetting, or replacing the Brownian motion with general Stationary process [58, 59], Lévy flights, fractional Brownian motion, continuous random walks [60–62] or active run-and-tumble particles. Another direction is adding an interaction into the system, and consider, for example noncrossing particles [63], ranked diffusion [64, 65] or Brownian particles with annihilation or coalescence [66]. Finally it would be interesting to step out of one dimension and ask all the questions mentioned above in two or three dimensions.

Appendix A: Comparison with the Local Time Density

As mentioned previously, the analysis we conducted in this paper to study the occupation time on the positive half-line is, in fact, very similar to the one performed in [3] for another Brownian functional: the local time density at the ori-

gin. Therefore, it is natural to present the results side by side and compare them, highlighting the similarities and differences between them. Below, we provide such a discussion.

Since we have used the notation T to denote both the occupation time on the positive half-line (in this paper) and the local time density at the origin (in [3]), to prevent confusion while comparing the results, we shall denote them by T^{occ} and T^{loc} respectively.

Both of the aforementioned observables belong to the class of additive Brownian functionals, and have the form

$$O = \sum_{i=1}^N \int_0^t V[x_i(t')] dt' \quad (\text{A1})$$

The difference between T^{occ} and T^{loc} lies in the choice of the functional $V[x(t)]$. Specifically, the occupation time on the positive half-line corresponds to $V[x(t)] = \theta[x(t)]$ whereas for the local time density $V[x(t)] = \delta[x(t)]$

$$T^{\text{occ}} \equiv \sum_i \int_0^t \theta[x_i(t')] dt', \quad (\text{A2})$$

$$T^{\text{loc}} \equiv \sum_i \int_0^t \delta[x_i(t')] dt'. \quad (\text{A3})$$

The occupation time quantifies how long particles reside in the positive half-line and it is exactly the *time* that the particles spent to the right of the origin. Since $\theta[x]$ is either 0 or 1, from (A2) it is evident, that if there are N particles in the system, then T^{occ} cannot be greater than Nt . In other words, its probability distribution is supported on the segment $[0, Nt]$.

$$\dim [T^{\text{occ}}] = \text{time}, \quad T^{\text{occ}} \in [0, Nt]. \quad (\text{A4})$$

The quantity T^{loc} in (A3), on the other hand, characterizes the amount of time particles have spent in the vicinity of the origin, but in a slightly more subtle way, as it is *time density* rather than time itself. Consequently, and this can be easily seen from (A3), the local time density is not bounded and can take arbitrarily large values.

$$\dim [T^{\text{loc}}] = \frac{\text{time}}{\text{length}}, \quad T^{\text{loc}} \in [0, \infty). \quad (\text{A5})$$

At first glance, these two observables appear quite similar. Indeed, since $\partial_x \theta(x) = \delta(x)$, they are related on the functional level. However, the reader should not let this similarity mislead them, since there is no straightforward way of deriving the results for one observable from those obtained for the other.

Nevertheless, we should mention that both T^{occ} and T^{loc} are special cases of another, more general, Brownian functional. Namely, if we choose $V[x(t)]$ to be an indicator function on a segment $[a, b]$,

$$V[x(t)] = \mathbb{1}_{[a,b]}[x(t)] \equiv \begin{cases} 1, & x(t) \in [a, b], \\ 0, & x(t) \notin [a, b], \end{cases} \quad (\text{A6})$$

then occupation time on the half-line and local time density at the origin may be interpreted as the following limits

$$T^{\text{occ}} = \lim_{\ell \rightarrow \infty} \sum_i \int_0^t \mathbb{1}_{[0,\ell]}[x_i(t')] dt', \quad (\text{A7})$$

$$T^{\text{loc}} = \lim_{\ell \rightarrow 0} \frac{1}{2\ell} \sum_i \int_0^t \mathbb{1}_{[-\ell,\ell]}[x_i(t')] dt'. \quad (\text{A8})$$

Thus, it would be interesting to study the Brownian functional with the potential (A6) and find the behavior of the corresponding probability distributions at large times. Then, by using (A7) and (A8) we could derive the results for T^{occ} and T^{loc} . However such a computation provide a challenging task, which falls beyond the scope of the present paper.

Let us now proceed and compare the results obtained for the occupation time on the positive half-line (which are summarized in Sec. II B) with those obtained by the authors previously in [3] for the local time density at the origin.

1. Typical values

First, let us have a look at the behaviors of the observables close to their typical values. In this case, both quenched and annealed probability distributions are Gaussian, and therefore we can describe them by first two cumulants: the mean and the variance.

The mean values for the quenched and annealed distributions are the same, and for T^{occ} and T^{loc} they are given by

$$\overline{\langle T^{\text{occ}} \rangle_{\mathbf{x}}} = \frac{2}{3} \sqrt{\frac{D}{\pi}} \bar{\rho} t^{3/2}, \quad \overline{\langle T^{\text{loc}} \rangle_{\mathbf{x}}} = \frac{1}{2} \bar{\rho} t. \quad (\text{A9})$$

For the variances in the quenched case we have

$$\text{Var}_{\text{qu}}[T^{\text{occ}}] = \frac{8(\sqrt{2}-1)}{15} \sqrt{\frac{D}{\pi}} \bar{\rho} t^{5/2} \quad (\text{A10})$$

$$\text{Var}_{\text{qu}}[T^{\text{loc}}] = \frac{2}{3} (2 - \sqrt{2}) \frac{1}{\sqrt{\pi D}} \bar{\rho} t^{3/2}, \quad (\text{A11})$$

and the annealed variances at large times behave as

$$\text{Var}_{\text{an}}[T^{\text{occ}}] \underset{t \rightarrow \infty}{\simeq} \frac{2}{5} \left[1 + \frac{(4\sqrt{2}-7)}{3} (1 - \alpha_{\text{ic}}) \right] \sqrt{\frac{D}{\pi}} \bar{\rho} t^{5/2}, \quad (\text{A12})$$

$$\text{Var}_{\text{an}}[T^{\text{loc}}] \underset{t \rightarrow \infty}{\simeq} \frac{2}{3} \left[1 + (1 - \sqrt{2}) (1 - \alpha_{\text{ic}}) \right] \frac{1}{\sqrt{\pi D}} \bar{\rho} t^{3/2}. \quad (\text{A13})$$

Note, that the scaling of the mean values and the variances of T^{occ} and T^{loc} are very different. For the local time density, the mean value grows as t and the variances grow as $t^{3/2}$, whereas for the occupation time the mean value grows as $t^{3/2}$ and the variances grow as $t^{5/2}$. Consequently, for studying the probability distributions in the large deviation formalism, we use different scaling variables, namely

$$\tau^{\text{occ}} = \frac{T^{\text{occ}}}{t^{3/2}} \frac{1}{\bar{\rho} \sqrt{4D}}, \quad \tau^{\text{loc}} = \frac{T^{\text{loc}}}{t} \frac{1}{\bar{\rho}}. \quad (\text{A14})$$

Let us emphasize, that the observables are very different (they even have different dimensions) and therefore there is no apparent reason for them to have the same scaling. However, there are still some similarities.

First, both for the occupation time and for the local time density, annealed variances depend on the initialization through the single static quantity α_{ic} (14), the Fano factor of the initial condition. Moreover for both observables, the dependence is linear. This is, in fact, expected, since the formalism we used in Sec. III B can be straightforwardly applied to any additive Brownian functional.

Second, the ratios between the square of the mean value and the variances are the same for T^{occ} and T^{loc} , namely

$$\frac{\left(\langle T^{\text{occ}} \rangle_{\mathbf{x}}\right)^2}{\text{Var}_{\text{an,qu}}[T^{\text{occ}}]} \underset{t \rightarrow \infty}{\sim} \frac{\left(\langle T^{\text{loc}} \rangle_{\mathbf{x}}\right)^2}{\text{Var}_{\text{an,qu}}[T^{\text{loc}}]} \underset{t \rightarrow \infty}{\sim} \bar{\rho} \sqrt{Dt}. \quad (\text{A15})$$

Hence the large deviation forms are

$$\mathbb{P}_{\text{an,qu}}[T^{\text{occ}}, t] \sim \exp \left[-\bar{\rho} \sqrt{4Dt} \Phi_{\text{an,qu}}(\tau^{\text{occ}}) \right], \quad (\text{A16})$$

$$\mathbb{P}_{\text{an,qu}}[T^{\text{loc}}, t] \sim \exp \left[-\bar{\rho} \sqrt{4Dt} \Phi_{\text{an,qu}}(\tau^{\text{loc}}) \right], \quad (\text{A17})$$

where an additional factor of 2 in the exponential, is due to purely esthetic reasons.

The factor $\bar{\rho} \sqrt{Dt}$ in (A16), (A17) is again very natural. The particles do not interact, hence both T^{loc} and T^{occ} are essentially sums of N independent random variables. However, a lot of these random variables are zeros. Indeed, only the particles that have reached the origin up to the observation time have nonzero contribution to both T^{occ} and T^{loc} . Since the typical displacement of a Brownian particle is proportional to \sqrt{Dt} , we expect, that the effective number of particles is proportional to $\bar{\rho} \sqrt{Dt}$. In other words, we have effectively $n \sim \bar{\rho} \sqrt{Dt}$ terms in (A2) and (A3), and therefore it is natural to expect this sums to be proportional to n . However, we should stress, that since we are dealing with nonidentically distributed random variables, the above argument is somewhat handwaving.

2. Atypical values

Now, let us comment on the tails of the probability distributions of T^{occ} and T^{loc} . Note, that if one observable is equal to zero, then the other one equals zero as well. This is simply

due to the fact, that both situations correspond to configurations of the trajectories in which no trajectory crosses the origin. Therefore we expect that $\mathbb{P}[T^{\text{loc}} = 0, t] \sim \mathbb{P}[T^{\text{occ}} = 0, t]$. This is in perfect agreement with our results,

$$\mathbb{P}_{\text{an}}[T^{\text{occ}} = 0, t] \sim \mathbb{P}_{\text{an}}[T^{\text{loc}} = 0, t] \sim e^{-\theta_{\text{an}} \bar{\rho} \sqrt{4Dt}} \quad (\text{A18})$$

$$\mathbb{P}_{\text{qu}}[T^{\text{occ}} = 0, t] \sim \mathbb{P}_{\text{qu}}[T^{\text{loc}} = 0, t] \sim e^{-\theta_{\text{qu}} \bar{\rho} \sqrt{4Dt}} \quad (\text{A19})$$

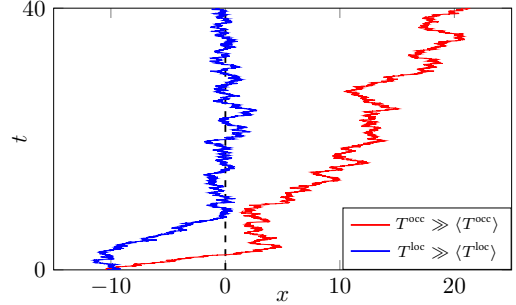


Figure 10. Examples of the Brownian trajectories with atypically large value of the occupation time (red) and local time density at the origin (blue). These two trajectories are qualitatively different. In the simulation $t = 40$, $x(0) = -10$, and $D = 1$. To obtain this picture, we have generated 10^7 independent Brownian trajectories and picked two of them corresponding to the largest values of T^{loc} and T^{occ} .

As for the atypically large values, the situation is different. Recall, that for the occupation time we have

$$\mathbb{P}_{\text{an}}[T^{\text{occ}}, t] \underset{T^{\text{occ}} \rightarrow \infty}{\sim} \exp \left[-\frac{T^{\text{occ}}}{2t} \log \left(\frac{(T^{\text{occ}})^2}{t^3 D \bar{\rho}^2} \right) \right], \quad (\text{A20})$$

$$\mathbb{P}_{\text{qu}}[T^{\text{occ}}, t] \underset{T^{\text{occ}} \rightarrow \infty}{\sim} \exp \left[-\frac{16}{27} \frac{T^{\text{occ}}}{t} \left(\frac{(T^{\text{occ}})^2}{t^3 D \bar{\rho}^2} \right) \right]. \quad (\text{A21})$$

whereas for the local time density

$$\mathbb{P}_{\text{an}}[T^{\text{loc}}, t] \underset{T^{\text{loc}} \rightarrow \infty}{\sim} \exp \left[-\sqrt{D} \frac{T^{\text{loc}}}{\sqrt{t}} \sqrt{\log \frac{T^{\text{loc}}}{t \bar{\rho}}} \right] \quad (\text{A22})$$

$$\mathbb{P}_{\text{qu}}[T^{\text{loc}}, t] \underset{T^{\text{loc}} \rightarrow \infty}{\sim} \exp \left[-\sqrt{\frac{32}{27}} \sqrt{D} \frac{(T^{\text{loc}})^{3/2}}{t \sqrt{\bar{\rho}}} \right], \quad (\text{A23})$$

There seems to be no similarity between the T^{loc} and T^{occ} but this should not surprise the reader. The trajectories, that contribute to the atypically large values of these observables are qualitatively different. This becomes clear when considering a single particle problem. Trajectories with $T^{\text{loc}} \gg \langle T^{\text{loc}} \rangle$ tend to remain close to the origin most of the time. On the other hand, trajectories with $T^{\text{occ}} \gg \langle T^{\text{occ}} \rangle$ can go arbitrary far from the origin (see Fig. 10).

-
- [1] B. Derrida and A. Gerschenfeld, Current Fluctuations in One Dimensional Diffusive Systems with a Step Initial Density Profile, *J. Stat. Phys.* **137**, 978 (2009), [arXiv:0907.3294](https://arxiv.org/abs/0907.3294).
 [2] P. L. Krapivsky and B. Meerson, Fluctuations of current in non-

stationary diffusive lattice gases, *Phys. Rev. E* **86**, 031106 (2012), [arXiv:1206.1842](https://arxiv.org/abs/1206.1842).

- [3] I. N. Burennev, S. N. Majumdar, and A. Rosso, Local time of a system of Brownian particles on the line with step-like initial

- condition, (2023), [arXiv:2306.16882](#).
- [4] N. R. Smith and M. Baruch, Macroscopic fluctuation theory of local time in lattice gases, (2023), [arXiv:2311.15286](#).
- [5] T. Banerjee, R. L. Jack, and M. E. Cates, Role of initial conditions in one-dimensional diffusive systems: Compressibility, hyperuniformity, and long-term memory, *Phys. Rev. E* **106**, L062101 (2022), [arXiv:2206.08739](#).
- [6] B. Sorkin and D. S. Dean, Single-file diffusion in spatially inhomogeneous systems, (2023), [arXiv:2306.10500](#).
- [7] D. S. Dean, S. N. Majumdar, and G. Schehr, Effusion of stochastic processes on a line, *J. Stat. Mech.* **2023**, 063208 (2023), [arXiv:2303.08961](#).
- [8] T. Banerjee, S. N. Majumdar, A. Rosso, and G. Schehr, Current fluctuations in noninteracting run-and-tumble particles in one dimension, *Phys. Rev. E* **101**, 052101 (2020), [arXiv:2001.01923](#).
- [9] S. Jose, A. Rosso, and K. Ramola, Generalized disorder averages and current fluctuations in run and tumble particles, (2023), [arXiv:2306.13613](#).
- [10] S. Jose, A. Rosso, and K. Ramola, Effect of initial conditions on current fluctuations in non-interacting active particles, (2023), [arXiv:2310.16811](#).
- [11] C. Di Bello, A. K. Hartmann, S. N. Majumdar, F. Mori, A. Rosso, and G. Schehr, Current fluctuations in stochastically resetting particle systems, *Phys. Rev. E* **108**, 014112 (2023), [arXiv:2302.06696](#).
- [12] A. K. Hartmann, S. N. Majumdar, and G. Schehr, The distribution of the maximum of independent resetting Brownian motions, (2023), [arXiv:2309.17432](#).
- [13] I. Bena and S. N. Majumdar, Universal extremal statistics in a freely expanding Jepsen gas, *Phys. Rev. E* **75**, 051103 (2007), [arXiv:cond-mat/0701130](#).
- [14] S. N. Majumdar, Brownian Functionals in Physics and Computer Science, *Curr. Sci.* **89**, 2076 (2005), [arXiv:cond-mat/0510064](#).
- [15] J. Lamperti, An occupation time theorem for a class of stochastic processes, *Trans. Amer. Math. Soc.* **88**, 380 (1958).
- [16] H. Kesten, Occupation times for Markov and semi-Markov chains, *Trans. Amer. Math. Soc.* **103**, 82 (1962).
- [17] A. N. Borodin and P. Salminen, *Handbook of Brownian Motion - Facts and Formulae* (Birkhäuser Verlag, Basel, 2002).
- [18] S. N. Majumdar and A. Comtet, Local and Occupation Time of a Particle Diffusing in a Random Medium, *Phys. Rev. Lett.* **89**, 060601 (2002), [arXiv:cond-mat/0202067](#).
- [19] S. Sabhapandit, S. N. Majumdar, and A. Comtet, Statistical properties of functionals of the paths of a particle diffusing in a one-dimensional random potential, *Phys. Rev. E* **73**, 051102 (2006), [arXiv:cond-mat/0601455](#).
- [20] T. Sadhu, M. Delorme, and K. J. Wiese, Generalized Arcsine Laws for Fractional Brownian Motion, *Phys. Rev. Lett.* **120**, 040603 (2018), [arXiv:1706.01675](#).
- [21] S. N. Majumdar and A. J. Bray, Large-deviation functions for nonlinear functionals of a Gaussian stationary Markov process, *Phys. Rev. E* **65**, 051112 (2002), [arXiv:cond-mat/0202138](#).
- [22] G. C. M. A. Ehrhardt, S. N. Majumdar, and A. J. Bray, Persistence exponents and the statistics of crossings and occupation times for Gaussian stationary processes, *Phys. Rev. E* **69**, 016106 (2004), [arXiv:cond-mat/0306101](#).
- [23] P. Singh and A. Kundu, Generalised ‘Arcsine’ laws for run-and-tumble particle in one dimension, *J. Stat. Mech.* **2019**, 083205 (2019), [arXiv:1906.09442](#).
- [24] H. J. O. Boutcheng, T. B. Bouetou, T. W. Burkhardt, A. Rosso, A. Zoia, and K. T. Crepin, Occupation time statistics of the random acceleration model, *J. Stat. Mech.* **2016**, 053213 (2016), [arXiv:1603.06883](#).
- [25] C. Godrèche and J. Luck, Statistics of the occupation time of renewal processes, *J. Stat. Phys.* **104**, 489 (2000), [arXiv:cond-mat/0010428](#).
- [26] S. Burov and E. Barkai, Residence Time Statistics for N Renewal Processes, *Phys. Rev. Lett.* **107**, 170601 (2011), [arXiv:1103.1142](#).
- [27] S. Burov and E. Barkai, Occupation Time Statistics in the Quenched Trap Model, *Phys. Rev. Lett.* **98**, 250601 (2007), [arXiv:cond-mat/0612667](#).
- [28] G. Bel and E. Barkai, Weak Ergodicity Breaking in the Continuous-Time Random Walk, *Phys. Rev. Lett.* **94**, 240602 (2005), [arXiv:cond-mat/0502154](#).
- [29] I. Dornic and C. Godrèche, Large deviations and nontrivial exponents in coarsening systems, *J. Phys. A: Math. Gen.* **31**, 5413 (1998), [arXiv:cond-mat/9712178](#).
- [30] T. J. Newman and Z. Toroczkai, Diffusive persistence and the “sign-time” distribution, *Phys. Rev. E* **58**, R2685 (1998), [arXiv:cond-mat/9804160](#).
- [31] A. Baldassarri, J. P. Bouchaud, I. Dornic, and C. Godrèche, Statistics of persistent events: An exactly soluble model, *Phys. Rev. E* **59**, R20 (1999), [arXiv:cond-mat/9805212](#).
- [32] P. Singh, Extreme value statistics and arcsine laws for heterogeneous diffusion processes, *Phys. Rev. E* **105**, 024113 (2022), [arXiv:2112.00088](#).
- [33] P. T. Nyawo and H. Touchette, A minimal model of dynamical phase transition, *EPL* **116**, 50009 (2017), [arXiv:1611.07707](#).
- [34] P. T. Nyawo and H. Touchette, Dynamical phase transition in drifted Brownian motion, *Phys. Rev. E* **98**, 052103 (2018), [arXiv:1808.06986](#).
- [35] F. den Hollander, S. N. Majumdar, J. M. Meylahn, and H. Touchette, Properties of additive functionals of Brownian motion with resetting, *J. Phys. A: Math. Theor.* **52**, 175001 (2019), [arXiv:1801.09909](#).
- [36] N. R. Smith, S. N. Majumdar, and G. Schehr, Striking universalities in stochastic resetting processes, *EPL* **142**, 51002 (2023), [arXiv:2301.11026](#).
- [37] A. Dhar and S. N. Majumdar, Residence time distribution for a class of Gaussian Markov processes, *Phys. Rev. E* **59**, 6413 (1999), [arXiv:cond-mat/9902004](#).
- [38] F. D. Stefani, J. P. Hoogenboom, and E. Barkai, Beyond quantum jumps: Blinking nanoscale light emitters, *Physics Today* **62**, 34 (2009).
- [39] Z. Toroczkai, T. J. Newman, and S. Das Sarma, Sign-time distributions for interface growth, *Phys. Rev. E* **60**, R1115 (1999), [arXiv:cond-mat/9810359](#).
- [40] S. N. Majumdar and D. S. Dean, Exact occupation time distribution in a non-Markovian sequence and its relation to spin glass models, *Phys. Rev. E* **66**, 041102 (2002), [arXiv:cond-mat/0207249](#).
- [41] A. C. Barato, E. Roldán, I. A. Martínez, and S. Pigolotti, Arcsine Laws in Stochastic Thermodynamics, *Phys. Rev. Lett.* **121**, 090601 (2018), [arXiv:1712.00795](#).
- [42] A. Clauset, M. Kogan, and S. Redner, Safe leads and lead changes in competitive team sports, *Phys. Rev. E* **91**, 062815 (2015), [arXiv:1503.03509](#).
- [43] V. Linetsky, Step options, *Mathematical Finance* **9**, 55 – 96 (1999).
- [44] H. Touchette, The large deviation approach to statistical mechanics, *Phys. Rep.* **478**, 1 (2009), [arXiv:0804.0327](#).
- [45] S. N. Majumdar and G. Schehr, Large deviations, ICTS Newsletter 3 (2017), [arXiv:1711.07571](#).
- [46] A. J. Bray, S. N. Majumdar, and G. Schehr, Persistence and first-passage properties in nonequilibrium systems, *Advances in Physics* **62**, 225 (2013), [arXiv:1304.1195](#).

- [47] B. Meerson, A. Vilenkin, and P. L. Krapivsky, Survival of a static target in a gas of diffusing particles with exclusion, *Phys. Rev. E* **90**, 022120 (2014), [arXiv:1406.3502](#).
- [48] P. Lévy, Sur certains processus stochastiques homogènes, *Compositio Mathematica* **7**, 283 (1940).
- [49] A. Erdélyi, W. Magnus, F. Oberhettinger, and F. G. Tricomi, *Higher transcendental functions*, Vol. 1 (McGraw-Hill Book Company, Inc., New York-Toronto-London, 1953).
- [50] R. Corless, G. Gonnet, D. Hare, D. Jeffrey, and D. Knuth, On the Lambert W-function, *Advances in Computational Mathematics* **5**, 329 (1996).
- [51] A. K. Hartmann, Sampling rare events: Statistics of local sequence alignments, *Phys. Rev. E* **65**, 056102 (2002), [arXiv:cond-mat/0108201](#).
- [52] A. K. Hartmann, Large-deviation properties of largest component for random graphs, *Eur. Phys. J. B* **84**, 627 (2011), [arXiv:1011.2996](#).
- [53] C. Nadal, S. N. Majumdar, and M. Vergassola, Statistical Distribution of Quantum Entanglement for a Random Bipartite State, *J. Stat. Phys.* **142**, 403 (2011), [arXiv:1006.4091](#).
- [54] A. K. Hartmann, P. Le Doussal, S. N. Majumdar, A. Rosso, and G. Schehr, High-precision simulation of the height distribution for the KPZ equation, *EPL* **121**, 67004 (2018), [arXiv:1802.02106](#).
- [55] U. Basu, S. N. Majumdar, A. Rosso, and G. Schehr, Long-time position distribution of an active Brownian particle in two dimensions, *Phys. Rev. E* **100**, 062116 (2019), [arXiv:1908.10624](#).
- [56] S. Redner, *A Guide to First-Passage Processes* (Cambridge University Press, 2001).
- [57] W. Krauth, *Statistical Mechanics Algorithms and Computations* (Cambridge University Press, 2006).
- [58] D. Nickelsen and H. Touchette, Anomalous Scaling of Dynamical Large Deviations, *Phys. Rev. Lett.* **121**, 090602 (2018), [arXiv:1803.05708](#).
- [59] B. Meerson, Anomalous scaling of dynamical large deviations of stationary Gaussian processes, *Phys. Rev. E* **100**, 042135 (2019), [arXiv:1909.01858](#).
- [60] W. Wang, E. Barkai, and S. Burov, Large Deviations for Continuous Time Random Walks, *Entropy* **22**, 697 (2020), [arXiv:2005.13174](#).
- [61] E. Barkai and S. Burov, Packets of Diffusing Particles Exhibit Universal Exponential Tails, *Phys. Rev. Lett.* **124**, 060603 (2020), [arXiv:1907.10002](#).
- [62] T. Samudrajit, A. Wyłomańska, G. Sikora, C. E. Wagner, D. Krapf, H. Kantz, A. V. Chechkin, and R. Metzler, Leveraging large-deviation statistics to decipher the stochastic properties of measured trajectories, *New J. Phys.* **23**, 013008 (2021), [arXiv:2005.02099](#).
- [63] S. Mukherjee and N. R. Smith, Dynamical phase transition in the occupation fraction statistics for non-crossing Brownian particles, *Phys. Rev. E* **107**, 064133 (2023), [arXiv:2303.17250](#).
- [64] P. Le Doussal, Ranked diffusion, delta Bose gas and Burgers equation, *Phys. Rev. E* **105**, L012103 (2021), [arXiv:2108.09515](#).
- [65] A. Flack, P. Le Doussal, S. N. Majumdar, and G. Schehr, Out of equilibrium dynamics of repulsive ranked diffusions: the expanding crystal, *Phys. Rev. E* **107**, 064105 (2023), [arXiv:2301.08552](#).
- [66] P. L. Krapivsky and E. Ben-Naim, Irreversible reactions and diffusive escape: stationary properties, *J. Stat. Mech.* **2015**, P05003 (2015), [arXiv:1503.04236](#).